

1 Influence of Tropospheric Temperature on the Formation and Aging of 2 Secondary Organic Aerosol from Biogenic Vapor Mixtures

3 *Linyu Gao*^{1,2,*}, *Stella E. I. Manavi*³, *Claudia Mohr*^{4,5}, *Junwei Song*^{1,2}, *Cheng Wu*⁶, *Thomas*
4 *Leisner*^{1,7}, *Spyros N. Pandis*³, and *Harald Saathoff*^{1*}

5 ¹ Institute of Meteorology and Climate Research, Karlsruhe Institute of Technology, Karlsruhe,
6 76344, Germany

7 ² Now at: Université Claude Bernard Lyon 1, CNRS, IRCELYON, Villeurbanne, 69626, France

8 ³ Department of Chemical Engineering, University of Patras, Patras, 26504, Greece

9 ⁴ Department of Environmental Systems Science, ETH, Zurich, 8092, Switzerland

10 ⁵ PSI Center for Energy and Environmental Sciences, Paul Scherrer Institute, Villigen, 5232,
11 Switzerland

12 ⁶ Department of Chemistry and Molecular Biology, University of Gothenburg, 41296,
13 Gothenburg, Sweden

14 ⁷ Institute of Environmental Physics, Heidelberg University, Heidelberg, 69120, Germany

15

16 Correspondence to: Linyu Gao (linyugao@163.com) & Harald Saathoff
17 (harald.saathoff@kit.edu)

18

19 Abstract

20 Atmospheric temperature and composition variations significantly influence secondary organic
21 aerosol (SOA) formation and aging, and thus fine particulate matter levels and properties
22 relevant for climate, air quality, and human health. However, the temperature dependence of
23 SOA formation and aging from mixed volatile organic compounds (VOCs) remains
24 insufficiently understood. Therefore, we investigated SOA formation from the oxidation of
25 isoprene and α -pinene mixtures covering the range of tropospheric temperatures (213 – 313 K).
26 We further examine the aging of the resulting SOA by gradually warming to mimic their
27 atmospheric transport and diurnal aging processes. Notably, at 213 K, isoprene most strongly
28 suppresses α -pinene dimer (C₁₈₋₂₀) formation, with isoprene- α -pinene cross dimers appearing
29 3.5 times more frequently than at 273 K, while the suppression is not temperature-sensitive
30 above 273 K. Upon subsequent warming, particles formed at different temperature ranges
31 undergo distinct aging processes including aerosol evaporation and water uptake. Surprisingly,
32 particles formed at higher temperatures are more oxidized yet more volatile than those formed
33 at lower temperatures and subsequently warmed. Chemical transport modeling accounting for
34 temperature-dependend simultaneous oxidation of isoprene and α -pinene predicts higher SOA
35 levels across Europe, aligning more closely with observations. These findings highlight the
36 need to consider both temperature and the interaction of biogenic VOCs to accurately describe
37 SOA formation, aging, and global burden.

38 1. Introduction

39 Aerosol particles are ubiquitous in the atmosphere, significantly impacting climate and having
40 adverse effects on air quality and human health (Paasonen et al., 2013; Mahowald, 2011; Aubry
41 et al., 2021). Organic aerosol (OA) makes up 20-90 % of the total fine particulate mass in the
42 troposphere (Jimenez et al., 2009). An important contributor to the global OA burden is
43 secondary organic aerosol (SOA), which emerges from the condensation of organic compounds
44 formed by the oxidation of volatile organic compounds (VOCs) (Kroll and Seinfeld, 2008).
45 Generally, the key precursors for global SOA are biogenic VOCs, of which isoprene (C_5H_8)
46 and monoterpenes ($C_{10}H_{16}$) are the most abundant (Kanakidou et al., 2005). Consequently, large
47 efforts (Kanakidou et al., 2005; Carlton et al., 2009; Kroll and Seinfeld, 2008; Zhang et al.,
48 2015; Hallquist et al., 2009; Lopez-Hilfiker et al., 2014; Mcfiggans et al., 2019; Takeuchi et al.,
49 2022) have been put into investigating their formation chemistry and particle physicochemical
50 properties of biogenic SOA.

51 Most of these studies were done at or near room temperature (Zhang et al., 2015; Lopez-Hilfiker
52 et al., 2015; Kourtchev et al., 2015; Takeuchi et al., 2022; Mcfiggans et al., 2019). The
53 troposphere however covers a wide temperature range between 310 K to 200 K. In the near-
54 surface atmosphere, VOCs can be oxidized at varying ambient temperatures throughout the day,
55 depending on the season and region. By convective systems, VOCs could reach to higher
56 altitudes where they can be oxidized at lower temperatures (Schulz et al., 2018; Liu et al., 2023).
57 This is important for the prediction of SOA levels especially in the free troposphere.
58 Temperature affects the reaction rates and pathways (Bilde et al., 2015; Bianchi et al., 2019) of
59 VOCs oxidation as well as the gas-to-particle partitioning of oxidation products (Sheehan and
60 Bowman, 2001; Donahue et al., 2006; Jonsson et al., 2008; Simon et al., 2020), thereby altering
61 the formation, chemical composition, and physicochemical properties of aerosol particles. Thus,
62 developing a comprehensive study covering tropospheric conditions is essential for
63 understanding SOA formation and aging processes in the real atmosphere.

64 Isoprene makes up the largest portion of the global biogenic VOC emissions (Owen et al., 2003;
65 Sindelarova et al., 2014), making it an important SOA precursor despite its relatively low
66 individual mass yield of <5% (Xu et al., 2014; Lamkaddam et al., 2021; Carlton et al., 2009).
67 Previously, Kiendler-Scharr et al. (2009) and Mcfiggans et al. (2019) found that at room
68 temperature, the presence of isoprene reduces SOA formation from the oxidation of α -pinene.
69 This is due to the competition of isoprene and α -pinene for reacting with hydroxyl radicals (OH)
70 (Mcfiggans et al., 2019) and the formation of more volatile C_{15} dimers from the reaction of C_{10}
71 peroxy radicals (RO_2) of α -pinene and C_5 RO_2 of isoprene, instead of less volatile C_{20} dimers
72 from self-reactions of C_{10} RO_2 from α -pinene alone. However, the temperature dependence of
73 RO_2 cross reactions in the isoprene and α -pinene systems as well as the effects of temperature
74 changes on SOA aging during atmospheric processes such as transport and diurnal aging
75 remains to be fully understood. This knowledge gap is critical given the varying atmospheric
76 abundances of these compounds across different ecosystems. For instance, in the Amazonian
77 rainforest, summertime isoprene mixing ratios range from 0.1 to 20 ppb (Yáñez-Serrano et al.,
78 2020; Yáñez-Serrano et al., 2018), while monoterpenes are typically below 1 ppb but can reach
79 up to 5.5 ppb. In contrast, European forests exhibit lower isoprene levels, typically below 1 ppb
80 but reaching up to ~5 ppb during warm daytime periods (Li et al., 2021; Petersen et al., 2023).
81 Monoterpene concentrations in these forests are also generally below 1 ppb but can reach
82 several tenths of ppb during summer across a typical temperature range of 10–35 °C (Li et al.,
83 2021). Therefore, investigating the impact of temperature on the oxidation of isoprene and α -

84 pinene mixtures at atmospherically relevant concentrations is essential to accurately predict
85 SOA formation in diverse environmental conditions (Tripathi et al., 2025; Curtius et al., 2024).

86 We thoroughly investigated the temperature-dependent formation and the properties of SOA
87 from the oxidation of the mixture of isoprene and α -pinene at 213 K (SOA_{213K}), 243 K
88 (SOA_{243K}), 273 K (SOA_{273K}), 298 K (SOA_{298K}), and 313 K (SOA_{313K}). The SOA formed at each
89 temperature was subsequently warmed with increments of 15-30 K over 10 hours to investigate
90 the aging processes (e.g., diurnal cycle) of SOA over a wider tropospheric temperature range
91 (i.e., SOA_{213K}→243K, SOA_{243K}→273K, SOA_{273K}→298K, and SOA_{298K}→313K). A series of cross dimers
92 from the two precursor VOCs were identified by making use of carbon isotope (¹³C) labelling
93 experiments, as well as by comparison with the sole α -pinene oxidation experiment. We
94 demonstrated the effect of temperature on the suppression of α -pinene dimers by isoprene and
95 the formation of two-precursor cross dimers. By studying the effect of warming on aged
96 particles, we distinguished the impact of temperature on both the chemistry and phase
97 partitioning of organic molecules and provided evidence that particles at different temperature
98 ranges undergo distinct aging processes (i.e., evaporation and water uptake) during warming.

99 2.Methods

100 2.1 Simulation Chamber Experiments

101 The data presented here was measured in two campaigns in 2019 (SOA19b) and 2021 (SOA21a)
102 covering 213 – 313 K in the Aerosol Interaction and Dynamics in the Atmosphere (AIDA)
103 aerosol and cloud simulation chamber at the Karlsruhe Institute of Technology (KIT). The
104 chamber is an 84.5 m³ aluminium vessel equipped with a LED solar radiation simulator and
105 with precisely controlled temperature, humidity, and gas mixtures. A fan allows all components
106 to be mixed well within 90 seconds (Saathoff et al., 2009). Details about the AIDA chamber
107 are given by previous studies (Möhler et al., 2003; Vallon et al., 2022; Wagner et al., 2006).

108 Two types of SOA were generated in batch mode from dark oxidation of: (1) sole α -pinene at
109 273 K (SOA_{ap-273}), (2) isoprene mixed with α -pinene at 213K, 243K, 273K, 298K, and 313K
110 (SOA_{213K}, SOA_{243K}, SOA_{273K}, SOA_{298K}, SOA_{313K}), respectively. The experimental conditions
111 are summarized in Table 1. Well defined amounts of isoprene and α -pinene were added to the
112 AIDA chamber with a flow of 10 L/min of synthetic air. Ozone was injected subsequently after
113 the biogenic VOC were mixed well inside the chamber, followed by the continuous addition of
114 tetramethyl ethylene (TME) generating OH radicals by its reaction with ozone. The OH
115 concentrations were $(0.8-1.5) \times 10^7$ molecules cm⁻³ in all experiments. The initial concentration
116 ratios of isoprene to α -pinene were kept at 1.0 ± 0.1 for all two-precursor experiments, while
117 the ratios of O₃ to α -pinene were 14 ± 3 among all experiments with the exception of Exp 1 at
118 213 K (O₃: α -pinene = 38). At 213 K, the initial concentrations of isoprene and α -pinene of 6.7
119 ppb led to a relatively small amount of SOA mass. To generate sufficient SOA mass for the
120 longer warming experiment we generated more SOA mass in a second oxidation step with about
121 twice the VOC concentrations of 13.5 ppb. We note that the two times of injections of
122 precursors may have impact on the chemical regimes during the SOA formation at 213 K
123 compared to other experiments. Seed particles and OH scavengers were not used in this work.
124 Additionally, to investigate the cross-dimers formed from the oxidation of α -pinene and
125 isoprene, we used ¹³C-labelled isoprene (>98%, Merck) in Experiments 6 and 7 (Table 1). This
126 isotopic labelling enabled us to identify products with a shift of one nominal mass-to-charge
127 unit (i.e., m/z +1), which unambiguously marks those dimers containing one skeleton from the
128 labelled isoprene.

129 The initial reaction lasted 90 minutes, then the VOC precursors were depleted. The subsequent
130 course of the experiment consisted of one hour of photochemical aging by illumination and then
131 14 hours of warming the entire chamber at a constant rate. The increment of temperature before
132 and after warming is shown in Table 1. To evaluate the effect of dilution, we injected CO₂
133 which is a chemistry bystander before warming. The loss of CO₂ was less than 4% for all
134 experiments after 14 h of warming. Therefore, the dilution effect is neglectable.

Table 1. Experimental conditions for SOA from sole α -pinene and mixtures of isoprene and α -pinene.

Exp No.	SOA type		Initial formation temperature [K]	RH before warming [%]	VOC conc. [ppb]		O ₃ [ppb]	Temperature during warming (start → end) [K]	RH after warming [%]	Newly formed SOA conc. [$\mu\text{g m}^{-3}$]	Particle Yield
	Before warming	After warming			α -pinene	isoprene					
0	SOA _{ap-273}	-	273	63	20.5	0	345	-	-	65.3	0.52
1	SOA _{213K}	SOA _{213K} → _{243K}	213	16	20.2	20.2	366*	213 → 243	4	-	-
2	SOA _{243K}	SOA _{243K} → _{273K}	243	80	25	25	367	243 → 273	6	132.5	0.48
3	SOA _{273K}	SOA _{273K} → _{298K}	273	58	21.5	20.8	371	273 → 298	12	81.9	0.46
4	SOA _{298K}	SOA _{298K} → _{313K}	298	28	31.3	28.6	355	298 → 313	10	41.5	0.20
5	SOA _{313K}	-	313	12	49.8	49.8	507	-	-	35.9	0.09
6	SOA _{ap-13C-iso-273}	-	273	61	20.8	23	353	273 → 298	-	-	-
7	SOA _{ap-13C-iso-298}	-	298	28	31.1	28	357	298 → 313	-	-	-

*Total amount of O₃ of 366 ppb is summed from two rounds of injections: 253 ppb at the first injection, and 113 ppb at the second injection.

136 2.2 Instrumentation

137 The concentrations of VOC and semi-volatile organic particles were measured by a Proton-
138 Transfer-Reaction-Time-of-Flight-Mass-Spectrometer coupled with a Chemical Analysis of
139 Aerosol Online (CHARON-PTR-ToF-MS, Ionicon Analytik GmbH) particle inlet.

140 Bulk SOA was online detected by a high-resolution time-of-flight Aerosol Mass Spectrometer
141 (HR-AMS, Aerodyne Inc.), while the particle-phase chemical composition of SOA at molecular
142 level was detected by a chemical ionization mass spectrometer (CIMS) coupled with a filter
143 inlet for gas and aerosols (FIGAERO) using iodide (I⁻) as reagent ions with 1 Hz time resolution
144 (Lopez-Hilfiker et al., 2014; Lee et al., 2014). The CIMS data presented in this work stems
145 from offline analysis. The filter samples were analyzed using a FIGAERO-iodide-CIMS. We
146 also note that the sensitivity of FIGAERO-iodide-CIMS is highly dependent on the
147 functionalities of the organic compounds and can vary by orders of magnitudes (Lopez-Hilfiker
148 et al., 2016; Lee et al., 2014; Riva et al., 2019). Therefore, the results shown in this work are
149 based on signal intensities but not mass concentrations. The detailed description of instruments,
150 filter sample collection, and data analysis are described in Section S1 and Figure S1.

151 O₃ was detected by a gas monitor (O₃41M, Environment SA). Particle size distributions and
152 number concentrations were measured by a scanning mobility particle sizer (SMPS) utilizing a
153 differential mobility analyzer (DMA, 3071 TSI Inc.) connected to a condensation particle
154 counter (CPC, 3772, TSI Inc.). The total particle number concentrations were monitored by two
155 condensation particle counters (CPC, 3776 and 3022A, TSI Inc.).

156 Typically, background measurements for both gas and particle phase are done before and after
157 the addition of VOC to identify any contaminations inside the chamber. Gas background
158 confirms that there were no significant gas-phase contaminations for all the experiments. Most
159 of the particle background signals were coming from filter matrix contaminations mainly due
160 to fluorinated constituents of low relevance. Please note that the background in all experiments
161 was measured in the same way as described previously (Gao et al., 2022).

162 2.3 Determination of SOA particle volatility and glass transition temperature (T_g)

163 The large number of organic compounds detected in the particle phase are presented in a one-
164 dimensional volatility basis set (1D-VBS) (Donahue et al., 2006), based on the effective
165 saturation concentration (C_{sat} , $\mu\text{g m}^{-3}$). In this work, 298 K C_{sat} ($C_{sat,298K}$, $\mu\text{g m}^{-3}$) values of
166 individual compounds are determined according to their measured elemental formulas applying
167 a parameterization using molecular corridors (Li et al., 2016). The saturation concentration of
168 species at other temperatures ($C_{sat,T}$, $\mu\text{g m}^{-3}$) can be derived from $C_{sat,298K}$ according to the
169 Clausius-Clapeyron relation:

$$170 \quad C_{sat,T} = C_{sat,298K} \exp\left(\frac{\Delta H_{vap}}{R} \left(\frac{1}{298} - \frac{1}{T}\right)\right) \quad (1)$$

171 where T is the experimental temperature in K; ΔH_{vap} is the evaporation enthalpy in kJ mol^{-1} ,
172 which can be estimated based on $C_{sat,298K}$ by (Stark et al., 2017)

$$173 \quad \Delta H_{vap} = -5.7 \times \log_{10} C_{sat,298K} + 129 \quad (2)$$

174 In the volatility basis set, we use the following volatility classes: ultra-low VOC (ULVOC,
175 $\log_{10} C_{sat} < -8.5$), extremely low VOC (ELVOC, $-8.5 < \log_{10} C_{sat} < -4.5$), low VOC (LVOC, -4.5
176 $< \log_{10} C_{sat} < -0.5$), semi VOC (SVOC, $-0.5 < \log_{10} C_{sat} < 2.5$), intermediate VOC (IVOC, $2.5 <$
177 $\log_{10} C_{sat} < 6.5$), and VOC ($\log_{10} C_{sat} > 6.5$). Based on the same dataset as the volatility prediction,

178 the glass transition temperature (T_g) of CHO compounds is estimated by the parameterization
179 method expressed by the equation (3) (Derieux et al., 2018):

$$180 \quad T_g = (n_C^0 + \ln(n_C))b_C + \ln(n_H) b_H + \ln(n_C) \ln(n_H) b_{CH} + \ln(n_O) b_O + \ln(n_C) \ln(n_O) b_{CO}$$

181 (3)

182 where n_C , n_H , n_O are the number of molecular C, H, O atoms, respectively; n_C^0 is the reference
183 carbon number; b_C , b_H and b_O refers to the contribution of each atom to T_g ; and b_{CH} and b_{CO}
184 are coefficients reflecting contributions from carbon–hydrogen and carbon–oxygen bonds,
185 respectively. The values of all parameters used can be found in the published paper (Derieux et
186 al., 2018).

187 2.4 Transport Model Simulations

188 The simulation chamber results are implemented to PMCAMx (Murphy and Pandis, 2009), a
189 chemical transport model (CTM) which utilizes the SOA volatility bases set approach (Lane et
190 al., 2008) to simulate the formation of secondary aerosol from biogenic and anthropogenic
191 VOCs. A brief description of PMCAMx is provided in Section S2 of the supplement. The
192 model-incorporated stoichiometric yields are based on the molecular composition of the
193 particles measured by FIGARO-CIMS. The volatility of the produced aerosol is determined
194 following the approach described in Section 2.3, however, to minimize the computational cost
195 the species are re-distributed to four VBS bins (10^0 , 10^1 , 10^2 , $10^3 \mu\text{g m}^{-3}$) rather than using the
196 whole volatility range. The stoichiometric yields of both isoprene and α -pinene are temperature
197 dependent based on the parameterization of Exp 1-5. Specifically: $T < 243 \text{ K}$, parameters based
198 on Exp1 (213 K); $243 \text{ K} \leq T < 273 \text{ K}$, parameters from Exp 2 (243 K); $273 \text{ K} \leq T < 298 \text{ K}$,
199 parameters from Exp 3 (273 K); $298 \text{ K} \leq T < 313 \text{ K}$, parameters from Exp 4 (298 K); $T \geq 313$
200 K, parameters from Exp 5 (313 K). For the partitioning of the secondary organic species
201 between the gas and the aerosol phase, PMCAMx assumes that there is equilibrium between
202 the two phases and that the organic compounds form a pseudo-ideal solution. Specifically, in
203 the model the partitioning of the organics between the gas and the aerosol phase depends on
204 two parameters, the temperature and the total OA concentration of the simulated cell. Therefore,
205 the model can replicate the concentration changes that occur in the atmosphere due to both
206 warming and cooling. Utilizing the experimental data after warming rather than before warming
207 commenced inside the chamber would result in the same predicted SOA concentrations by
208 PMCAMx. Nevertheless, the warming stage of the experiments is better represented in the
209 model by adopting the mass-stoichiometric yields derived from the initial temperatures. Values
210 for the Base and New cases are provided in Table S1 and S2. Utilizing the stoichiometric yields
211 of Table S2, Figure S2 depicts the secondary organic aerosol mass fraction derived as a function
212 of the total organic aerosol mass together with the experimentally measured values.

213 The period considered in this model application is 5 June – 8 July 2012 (PEGASOS campaign)
214 in a European domain ($5400 \times 5832 \text{ km}^2$, Figure S3 and S4) with $36 \times 36 \text{ km}$ grid resolution,
215 and 14 vertical layers extending up to 7.5 km above ground. The temperature together with
216 other metrological parameters are provided by the Weather Research and Forecasting
217 meteorological model (WRF). Biogenic emissions are calculated by the MEGAN model
218 (Guenther et al., 2006), while anthropogenic and wildfire emissions are based on the GEMS
219 (Visschedijk et al., 2007) and IS4FIRES (Sofiev et al., 2008) inventories, respectively. In our
220 application, the domain average concentrations of isoprene and terpene in the simulated
221 European domain are 0.15 ppb and 0.04 ppb, respectively, with maximum predicted values of

222 2.8 ppb and 0.5 ppb. The spatial distributions of their average ground-level concentrations over
223 Europe are showed in Figure S3.

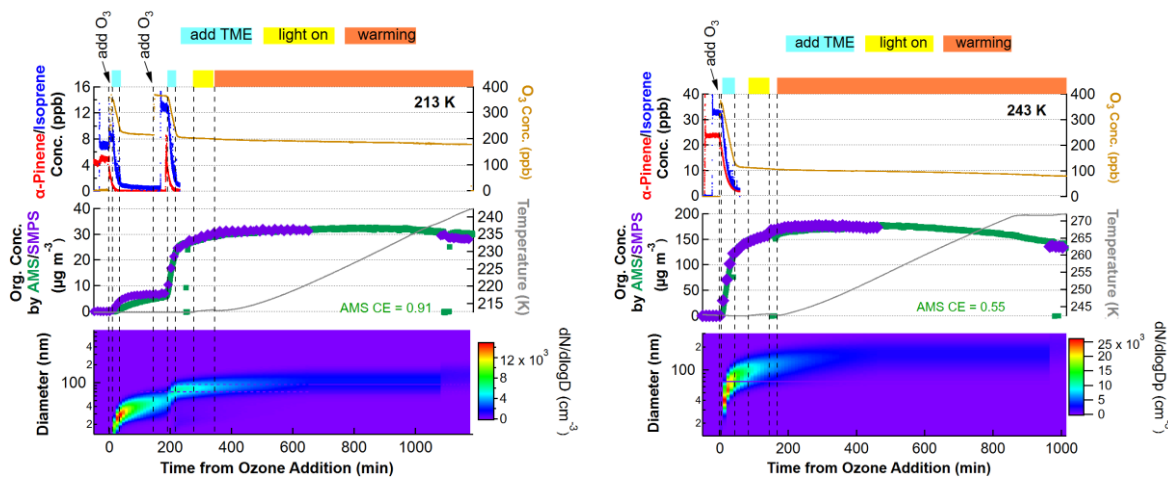
224 **3.Results**

225 **3.1 Influence of temperature on particle-phase chemical composition**

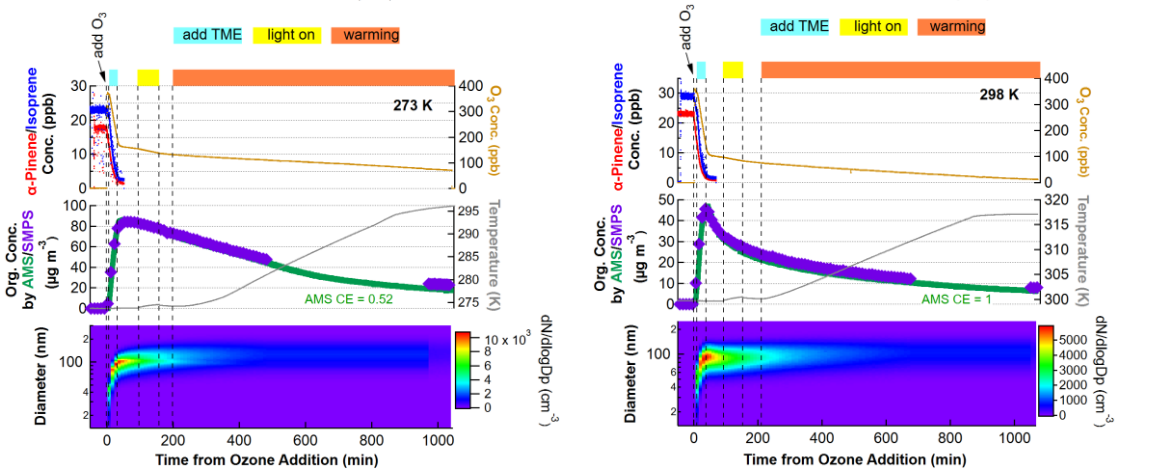
226 In each experiment, the molecular composition of fresh SOA particles was characterized by
227 FIGAERO-iodide-CIMS using iodide as the reagent ion. The evolution of trace gases as well
228 as particle mass and size distribution for the oxidation of isoprene α -pinene mixture at all
229 temperatures are shown in Figure 1. The beginning of the ozone addition is considered time
230 zero for each experiment. The addition of ozone and the subsequent production of OH radicals,
231 resulted in the complete depletion of the initial α -pinene and isoprene. The SOA particle
232 diameters increased typically to 65-100 nm and the mass concentrations of the newly formed
233 SOA ranged between 33-133 $\mu\text{g m}^{-3}$ (mass yield: 9-52 %) depending on temperature.
234 Subsequently, the fresh SOA was exposed to simulated solar radiation for 1 h. This
235 photochemical aging resulted in no significant chemical change (cf. Figure S9). This aging age
236 was followed by 10-12 h of warming, which will be discussed in Section 3.2.

237 We present first the identified cross dimers formed from concurrent oxidation of isoprene and
238 α -pinene (hereafter 'ISO-AP dimers') at 273 K. By comparison of the particle-phase chemical
239 composition among the experiment for sole α -pinene (Exp 0), α -pinene and isoprene mixture
240 at an equal concentration (Exp 3), and α -pinene and ^{13}C labelled isoprene mixture at an equal
241 concentration (Exp 6) shown in Table 1, we identified ISO-AP dimers such as $\text{C}_{15}\text{H}_{20}\text{O}_{3-7}$,
242 $\text{C}_{15}\text{H}_{22}\text{O}_{3-9}$, $\text{C}_{15}\text{H}_{24}\text{O}_{4-9}$, $\text{C}_{15}\text{H}_{26}\text{O}_{5-9}$, $\text{C}_{15}\text{H}_{28}\text{O}_{5-9}$, $\text{C}_{14}\text{H}_{20}\text{O}_{6-8}$, $\text{C}_{14}\text{H}_{22}\text{O}_{5-9}$, and $\text{C}_{14}\text{H}_{24}\text{O}_{6-8}$. The
243 identification of these cross dimers with 3-9 oxygen atoms completes the list of highly
244 oxygenated cross dimers with 9-13 oxygen atoms, which were previously identified by a CIMS
245 using nitrate as the reagent ion (Mcfiggans et al., 2019; Heinritzi et al., 2020). Among all
246 identified ISO-AP C_{14-15} cross dimers in Exp 3, $\text{C}_{15}\text{H}_{24}\text{O}_{4-9}$ and $\text{C}_{14}\text{H}_{22}\text{O}_{5-9}$ contribute most to
247 the total signals (21 %), followed by $\text{C}_{15}\text{H}_{26}\text{O}_{5-9}$, $\text{C}_{15}\text{H}_{28}\text{O}_{5-9}$, and $\text{C}_{15}\text{H}_{22}\text{O}_{3-9}$ with signal
248 fractions of 16 %, 11 %, and 11 %, respectively. The relative abundances of these cross dimers
249 in Exp 0 and Exp 6 are given in Figures S5-S6. Due to the scavenging of OH and RO_2 radicals
250 in the presence of isoprene, the relative contribution of solely α -pinene derived C_{18-20} dimers
251 from ozonolysis increases, while the contribution of dimers formed via OH radical reactions
252 decrease (Figure S7). This is qualitatively consistent with previous studies (Mcfiggans et al.,
253 2019; Heinritzi et al., 2020; Wang et al., 2021) performed at ~ 298 K.

254



255



256 Figure 1. Evolution of trace gases as well as particle mass and size for the oxidation of isoprene and α -
 257 pinene mixtures at 213 K, 243 K, 273 K, and 298 K. The time axis is relative to the first addition of
 258 ozone. The top shaded area of each plot shows the addition of TME to form OH radicals (blue), light on
 259 (yellow), as well as warming period (orange).

260 As shown in Figure 2, particle-phase C₁₄₋₁₅ ISO-AP cross dimers show higher signal fractions
 261 at lower temperatures (in all detected compounds, 16% and 11% in total for 213 K and 243 K,
 262 respectively) compared to those formed at higher temperatures (<4 % for 273 K, 298 K, and
 263 313 K). For the dimers formed from α -pinene oxidation alone (C₁₈₋₂₀, hereafter ‘AP-AP
 264 dimers’), including those from self- (i.e., both RO₂ involved in the dimerization originate either
 265 from O₃ oxidation or from OH oxidation.) and cross-dimerization (i.e., between the two RO₂
 266 radicals involved in the dimerization, one originates from O₃ oxidation, while the other
 267 originates from OH oxidation) of RO₂ derived from α -pinene oxidation initiated by both O₃ and
 268 OH radicals, lower temperatures exhibit slightly higher fractions with 8% - 9% at 213 – 243 K
 269 compared to 4% - 6% at 273 – 313 K, consistent with previous observations (Zhang et al., 2015).
 270 Most interestingly, the ratio of ISO-AP dimers to AP-AP dimers is 3.5 times higher at 213 K
 271 (the ratio is 2) than that at 273 – 313 K (the ratios are 0.6, Figure 2f). This indicates that the
 272 production of ISO-AP dimers plays a progressively more important role in SOA formation at
 273 lower temperatures. Shown as Figure 2g and 1h, the higher ratio of ISO-AP dimers to AP-AP
 274 dimers at 213 K than 313 K is mainly contributed by the greater formation of C₁₄₋₁₅ compounds.
 275 The volatility (expressed by the saturation concentration at 298 K, C_{298K}^{*}) of ISO-AP dimers
 276 (C_{298K}^{*}: 10^{-3.6}-10^{2.2} $\mu\text{g m}^{-3}$) is generally higher than that of AP-AP dimers (C_{298K}^{*}: 10^{-4.8}-10^{0.6}
 277 $\mu\text{g m}^{-3}$), indicating that ISO-AP dimers are more volatile than AP-AP dimers when formed at

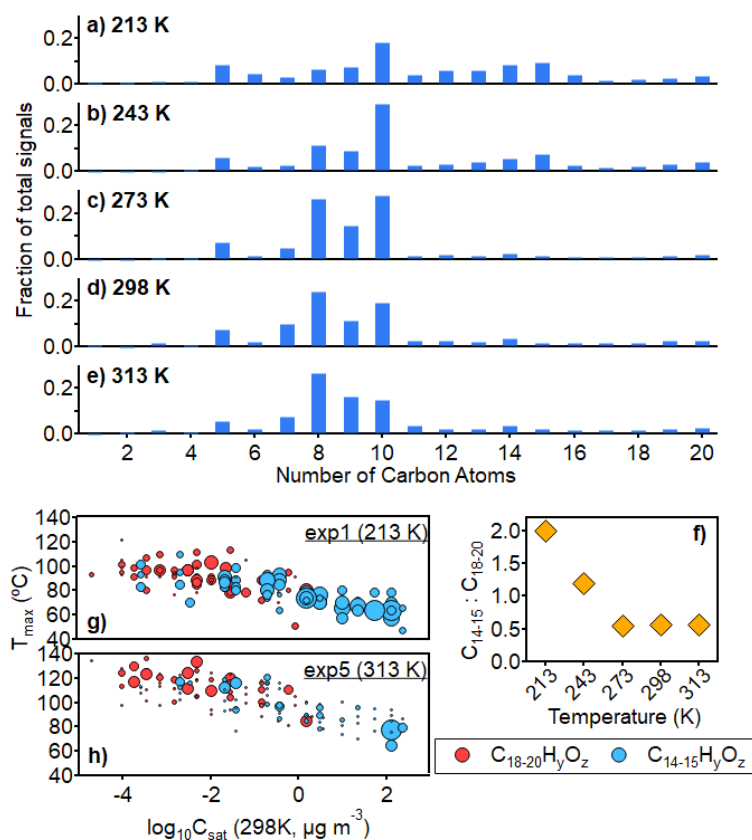
278 the same low temperatures. The difference in volatility between both groups of dimers is also
279 shown by their desorption temperature of maximum signal in the FIGAERO thermograms
280 (hereafter ' T_{\max} ') (Lopez-Hilfiker et al., 2014), which is an independent and qualitative
281 indicator of effective volatility compared to the volatility estimated by the parameterization
282 approach (Li et al., 2016) used in this work (Section S3, Figure S8).

283 Figure 3 shows the comparison of the particle volatility distribution at different temperatures.
284 This comparison integrates two approaches: gas- and particle-phase measurements at each
285 temperature (i.e., $C^* = C_{OA} \frac{G_i}{P_i}$ (Gkatzelis et al., 2018)) and the Clausius–Clapeyron equation.

286 C_{14-15} dimers span in the less volatile bins from Clausius-Clapeyron equation at temperatures
287 below 273 K, exhibiting a strong temperature dependence, compared with the volatility based
288 on the measured organic mass. This dependence is suggested to be chemistry-driven rather than
289 governed solely by phase partitioning. We interpret this as follows. First, the gas-phase
290 production rates of the two types of dimers may be temperature dependent due to the
291 temperature-affected concentrations of RO_2 radicals. The gas-phase dimer formation rate via
292 the bimolecular termination of $RO_2 + R'O_2 \rightarrow ROOR'$ rises strongly with temperature
293 (Quéléver et al., 2019). At lower temperatures, the lower rate coefficient of α -pinene + O_3
294 (Khamaganov and Hites, 2001; Bernard et al., 2012) and higher rate coefficient of isoprene +
295 OH (Campuzano-Jost et al., 2000; Campuzano-Jost et al., 2004; Dillon et al., 2017) lead to
296 higher differential between the concentrations of $C_{10} RO_2$ from α -pinene and $C_5 RO_2$ from
297 isoprene. Therefore, at lower temperatures, higher $[C_5 RO_2][C_{10} RO_2]$ results in larger
298 production of ISO-AP dimers compared with less formation of C_{20} AP-AP dimers due to lower
299 $[C_{10} RO_2][C_{10} RO_2]$. Besides, the other well-established dimer formation pathway for α -pinene
300 derived dimers, condensed-phase combination of acetyl peroxy radicals yielding diacyl
301 peroxides and their subsequent decomposition (Zhang et al., 2015) to produce esters, carboxylic
302 acids, and alcohols, is affected by temperature as well (Leffler and More, 1972; Lamb et al.,
303 1965). Our observation suggests that the formation of ISO-AP dimers via the diacyl peroxides
304 pathway may be faster than that of AP-AP dimers at lower temperatures. Second, previous
305 studies (Trump and Donahue, 2014; Morino et al., 2020) have shown that the decomposition
306 rates of dimers depend on temperature and the type of dimers. Therefore, we cannot exclude
307 that AP-AP dimers decompose faster than ISO-AP dimers at lower temperature, leading to
308 higher condensed-phase ratios of C_{14-15}/C_{18-20} .

309 It should be noted that the sensitivity of iodide chemical ionization exhibits substantial
310 variability in detecting organic compounds with different functional groups. As a result, signal-
311 based analyses may not accurately represent the actual abundances of these species.
312 Nevertheless, comparing signal fractions across different experiments can provide valuable
313 insights into product distributions and underlying reaction mechanisms.

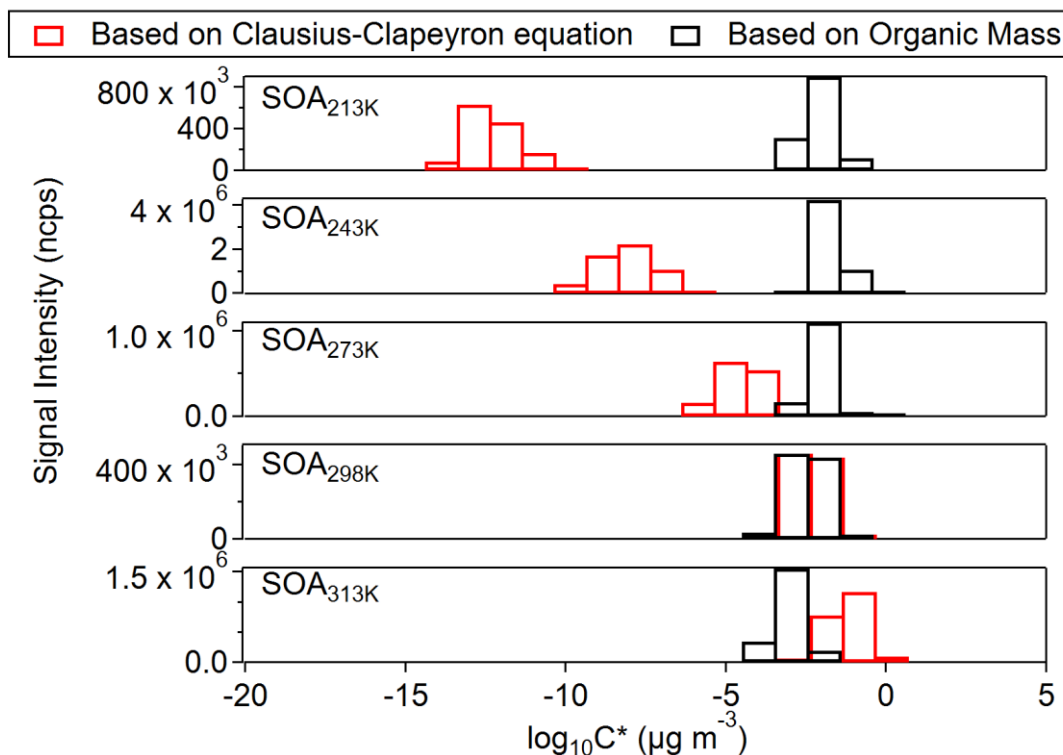
314 Overall, the nonmonotonic temperature dependence (Figure 2f) of the ratio of C_{14-15} to C_{18-20}
315 dimers between 213 – 313 K highlights the importance of the AP-AP dimer suppression by the
316 ISO-AP cross dimers. This is particularly relevant for biogenic particle formation and growth
317 in the real atmosphere especially at lower temperatures (Fu et al., 2009; Andreae et al., 2018).



318

319 Figure 2. Chemical composition of SOA derived from the mixture of isoprene and α -pinene at all
 320 temperatures (Exp 1-5): 213 K (a), 243 K (b), 273 K (c), 298 K (d), and 313 K (e); the ratio of C_{14-15}
 321 compound signals to C_{18-20} compound signals as a function of temperature (f); the distribution of C_{14-15}
 322 compounds and C_{18-20} compounds with molecular T_{max} corresponding to molecular logarithmic 298 K
 323 saturation concentration for Exp 1 at 213 K (g) and Exp 5 at 313 K (h). Sizes of symbols in (g) and (h)
 324 correspond to the normalised signal abundance of molecules.

325



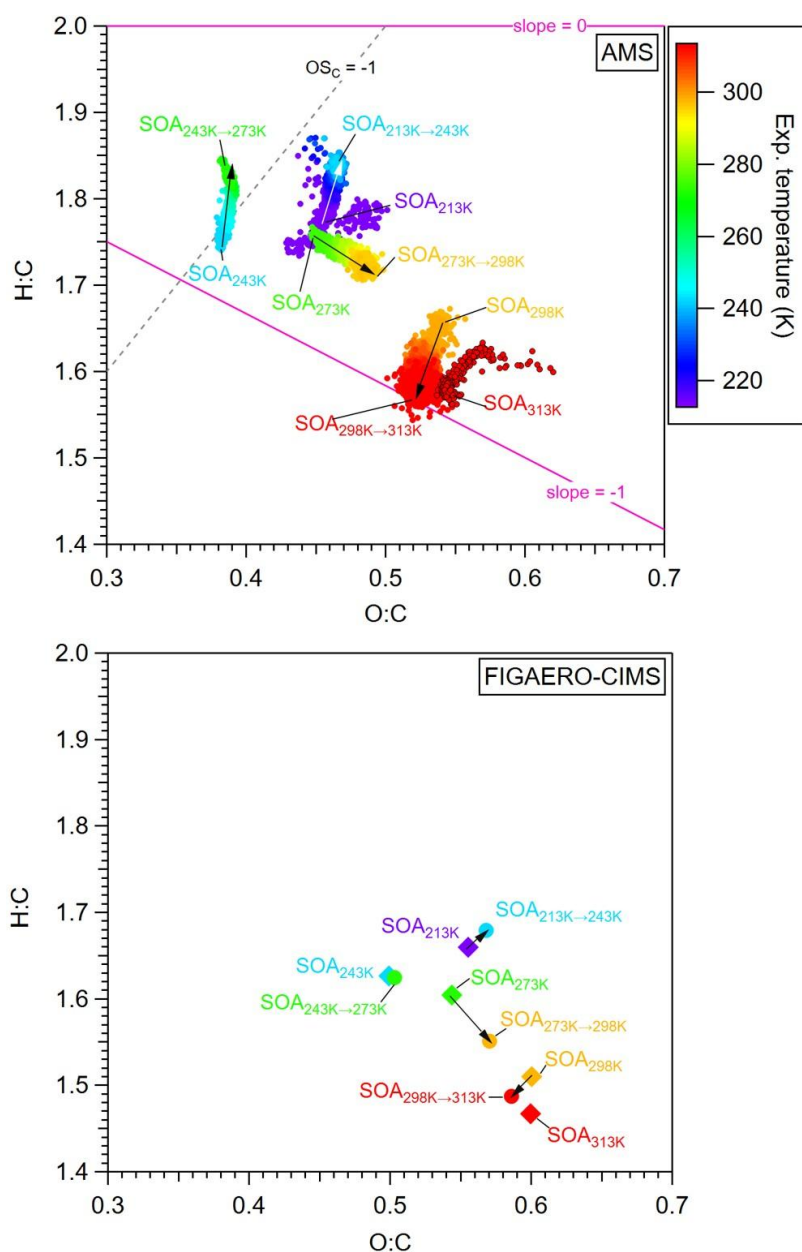
326

327 Figure 3. Volatility of C_{14-15} cross dimers formed at all temperatures calculated based on two approaches:
 328 $C_{OA} \frac{G_i}{P_i}$ (Gkatzelis et al., 2018) and Clausius-Clapeyron equation. The volatility of the bins is at their
 329 experiment temperatures.

330 3.2 Influence of temperature on SOA aging

331 To study the influence of temperature change on SOA formed at a specific temperature, we
 332 warmed the fresh SOA particles up by 1.4-2.4 K/h over 10-12 hours, which resembles the
 333 ambient temperature changing rate ($\sim 0.1-2$ K/h) in the real atmosphere (Hansen et al., 2006).
 334 The illumination has no significant effect on the bulk O:C, H:C and OS_C (Figure S9). The
 335 molecular chemical composition and volatility of fresh particles before warming are described
 336 in the Supplementary Section S3. Most interestingly, by warming, SOA particles formed
 337 initially at different temperatures showed distinct increments and/or decrements in bulk O:C
 338 and H:C ratios as well as oxidation states (OS_C) as measured by HR-AMS (Figure 4, Figure
 339 S10, and Table S3). It indicates these SOA particles underwent distinct aging processes
 340 including water uptake and evaporation when being warmed up.

341



342
 343 Figure 4. Van-Krevelen diagram for SOA particles during the warming periods of Exp 1 (213 K to 243
 344 K), Exp 2 (243 K to 273 K), Exp 3 (273 K to 298 K), Exp 4 (298 K to 313 K), and Exp 5 (313 K) from
 345 HR-AMS measurements (left) and FIGAERO-iodide-CIMS measurements mean values (right, symbols
 346 of diamonds and circles for warming start and end, respectively). Arrows are for guiding from the start
 347 to end of the warming periods. Symbols are coloured by temperatures. The carbon oxidation state ($OS_C = 2 O:C - H:C$)
 348 is shown with a grey dashed line. The pink lines with different slopes represent various
 349 reaction pathways: slope = 2 (hydration); slope = 0 (formation of hydroxy/peroxy groups); slope = -1
 350 (formation of carboxylic acids, or addition of both hydroxy and carbonyl groups).

351 We observed a clear increase of O:C ratios (from 0.36 to 0.54 from HR-AMS measurements,
 352 from 0.5 to 0.6 from FIGAERO-iodide-CIMS measurements) of fresh SOA particles formed
 353 between 243 K and 313 K (Figure 4). One exception is the particles formed at 213 K. The O:C
 354 ratio of the fresh SOA_{213K} (0.45 from HR-AMS measurement, 0.55 from FIGAERO-iodide-
 355 CIMS measurement) is higher than that of SOA_{243K}, contrary to the lower O:C ratios of particles
 356 formed at lower temperatures. This may result from the higher ratios of initial O₃ to VOCs
 357 concentrations (~19) in Exp 1 at 213K compared to other experiments (~7) (details in Method).

358 According to the HR-AMS measurements, the bulk O:C and H:C ratios of SOA particles
359 formed at 243 K (SOA_{243K}) increases from 0.36 to 0.4 and from 1.69 to 1.82, respectively,
360 during gradual warming to 273 K (SOA_{243K→273K}). Although the incremental O:C change is
361 small, the online HR-AMS measurements showed a significant trend during the warming
362 process (Figure 4). The ratio (=3.25) of the H:C increment and O:C increment in the Van-
363 Krevelen diagram indicates hydration reactions during warming (Schilling Fahnstock et al.,
364 2015; Heald et al., 2010). Correspondingly, the oxidation state (OS_C) of bulk SOA_{243K} decreases
365 from -0.97 to -1.02 for SOA_{243K→273K} (Figure S10), while the organic particle mass decayed 17%
366 as measured by HR-AMS. According to the FIGAERO-iodide-CIMS measurements, 18 %
367 fraction of the particle-phase C_xH_yO_z signals are lost during warming of SOA from 243 K
368 (SOA_{243K}) to 273 K (SOA_{243K→273K}) (Figure 5d). The loss of oxygenated organic compounds
369 mainly involves C₅, C₈₋₁₀, and C₁₄₋₁₅ compounds (Figure 5h), which are identified as monomeric
370 products from sole isoprene and sole α -pinene, and their ISO-AP dimers, respectively. However,
371 the loss of these oxygenated organic compounds leads to no significant change in the H:C ratio
372 (from 1.63 to 1.62) and O:C ratio (from 0.50 to 0.50) of the particle-phase C_xH_yO_z measured
373 by FIGAERO-iodide-CIMS. Therefore, the increase in bulk O:C and H:C ratios of SOA
374 measured by HR-AMS indicates not only hydration reactions (Schilling Fahnstock et al., 2015;
375 Heald et al., 2010) but also potential losses of more oxidized compounds with low H:C ratios.
376 The bulk SOA aging towards higher H:C and O:C ratios during warming is likely due not only
377 to sample evaporation but also to the change in the particle phase state.

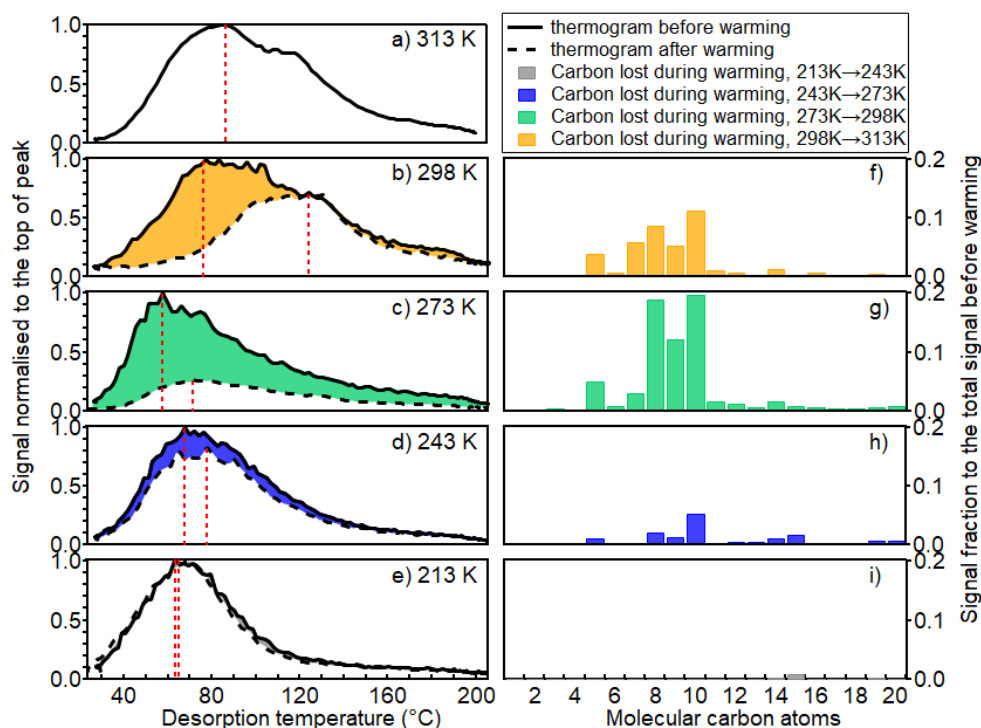
378 Similar changes of O:C and H:C ratios were observed for SOA_{213K} warmed to SOA_{213K→243K}.
379 Therefore, the SOA_{213K} warmed to SOA_{213K→243K} seems to undergo similar aging processes like
380 SOA_{243K} being warmed to SOA_{243K→273K}.

381 We characterized the viscosity of SOA particles by using the glass transition temperature, T_g
382 which is defined as the temperature at which an amorphous material transitions from a liquid-
383 like or semi-solid state to a glassy solid state. As the ambient temperature approaches or drops
384 below the T_g of a particle, its viscosity increases dramatically, often by several orders of
385 magnitude. Therefore, the phase state and viscosity of SOA can be inferred by characterizing
386 the T_g values. T_g was calculated for all detected organic compounds by FIGAERO-iodide-CIMS
387 using a parameterization approach (Derieux et al., 2018). In this study, SOA_{243K} is estimated to
388 be in a glassy solid state with a T_g of 289 K, comparable to the T_g values for sole isoprene- or
389 α -pinene-derived SOA reported in previous studies (Derieux et al., 2018; Ladino et al., 2014).
390 We note that the T_g values may be underestimated, as the water content in the particles was not
391 taken into account due to a lack of measurements. The high viscosity at low temperature
392 kinetically inhibits the diffusion of water and large organic molecules within the particle. Upon
393 warming, the particle transitions from a glassy to a semi-solid or liquid state, which facilitates
394 the uptake and internal mixing of water. This process can promote aqueous-phase reactions
395 (e.g., hydrolysis, oxidation) that alter the organic composition, increasing the H:C and O:C
396 ratios. Therefore, water uptake and the potential change of particle hygroscopicity (Shiraiwa et
397 al., 2017; Pajunoja et al., 2015; Shiraiwa et al., 2011) may contribute to increasing H:C and
398 O:C ratios of bulk SOA_{243K} during warming from 243 K to 273 K.

399 In contrast, from the HR-AMS measurement, the bulk SOA_{273K} loses 75% of mass, and show a
400 significant increase of OS_C (from -0.87 to -0.75) and O:C ratios (from 0.44 to 0.48) but a
401 decrease of H:C ratios (from 1.76 to 1.73) during warming to 298 K (Figure 4). This tendency
402 is consistent with the changes of O:C ratios and H:C ratios for the oxygenated constituents

403 measured by FIGAERO-iodide-CIMS. During warming of SOA_{273K} to 298 K, 72.5 % of all
 404 particle-phase C_xH_yO_z compounds are lost, with OS_C increasing from -0.52 to -0.41, O:C from
 405 0.54 to 0.57, and H:C ratios decreasing from 1.60 to 1.55. This indicates that evaporation is the
 406 main loss process with higher losses of less oxidized compounds. This is consistent with the
 407 analysis of HR-AMS spectra before and after warming (Figure S11) The T_g we estimated for
 408 SOA_{273K} is 278 K, which is in between the temperatures of warming at the start (273 K) and at
 409 the end (298 K). Therefore, the diffusion and evaporation of organic molecules are gradually
 410 less hindered when particle phase state transits from solid/semi-solid to liquid.

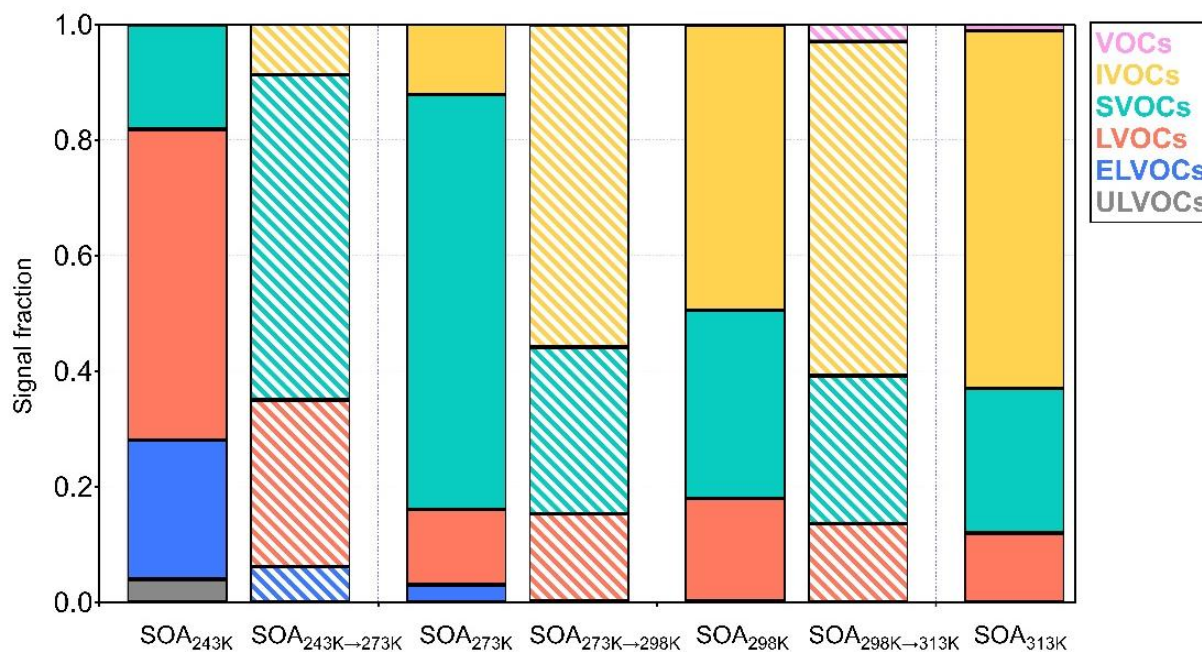
411 For the bulk SOA_{298K}, its estimated T_g is 283 K, which is evidently lower than the temperatures
 412 during warming from 298 K to 313 K. This indicates that the SOA_{298K} remain in the liquid
 413 phase during the whole warming process. As illustrated in Figure 4, warming of all SOA
 414 compounds formed at 298 K leads to lower H:C (from 1.63 to 1.57) and O:C ratios (weekly
 415 from 0.53 to 0.52), resulting in slightly higher OS_C values (from -0.57 to -0.53). During
 416 warming from 298 to 313 K, 40.2 % of all particle-phase C_xH_yO_z compounds and 71 % of
 417 organic particle mass were lost, by substantial evaporation. However, the evaporation induces
 418 only small changes of O:C ratio from 0.60 (SOA_{298K}) to 0.59 (SOA_{298K}→313K), H:C ratio from
 419 1.51 to 1.49, and OS_C from -0.31 to -0.32 for oxygenated organics, even though the trend is
 420 clear as shown in Figure 4. As the reduction in H:C ratio is around 2 times higher than the
 421 reduction in O:C ratio for bulk SOA_{298K} particles during the warming to 313 K, we infer that
 422 there might be water evaporation due to the potential particle-phase dehydration reactions
 423 involving elimination of H₂O.



424
 425 Figure 5. FIGAERO-iodide-CIMS thermograms of particles before and after warming process for all
 426 experiments ((a) for 313 K, (b) for 298 K, (c) for 273 K, (d) for 243 K, and (e) for 213 K), and the
 427 corresponding carbon distributions of molecules lost during warming (f-i). Black solid and dashed lines
 428 show the thermograms of particles sampled before and after warming, respectively. The thermograms
 429 are normalized to the peak signals of each thermogram before warming. Red vertical dashed lines
 430 indicate the T_{max} .

431 As illustrated in Figure 5, before warming, volatility indicated by the T_{\max} of the fresh particles
 432 showed a non-monotonic trend. This is similar with previous findings in the β -caryophyllene
 433 system (Gao et al., 2023), which is due to favoured condensation or oligomerization reactions
 434 at lower temperature and less production of low volatile HOMs which show larger fractions at
 435 warmer temperatures. During warming, the volatility of the particles is influenced by changes
 436 in their chemical composition as the gas-particle equilibrium is re-established through phase
 437 partitioning. As the temperature increases, more volatile organic compounds evaporate from
 438 the particle phase. Consequently, the particle composition becomes enriched in the remaining
 439 lower-volatile organic species. This is corroborated by the higher T_{\max} values observed in the
 440 thermograms: SOA_{243K→273K} (78 °C) compared to SOA_{243K} (68 °C), SOA_{273K→298K} (71 °C)
 441 compared to SOA_{273K} (57 °C), and SOA_{298K→313K} (124°C) compared to SOA_{298K} (77 °C), as
 442 illustrated in Figure 5b-d. The results indicate that the overall effect of warming on the SOA
 443 particle volatility is governed by the initial temperature-dependent chemical composition and
 444 the corresponding glass transition temperature.

445 Further support comes from the distribution of volatility groups estimated by the
 446 parameterization approach (Li et al., 2016) based on measured numbers of molecular carbon,
 447 hydrogen, and oxygen atoms. During warming, evaporation leads to compositional changes that
 448 enrich the relatively lower-volatility compounds. Concurrently, rising temperatures shift the
 449 entire VBS toward higher apparent volatility, following the Clausius-Clapeyron relation. For
 450 instance, despite the evaporation of some volatile components during warming from 243 K to
 451 273 K, the resulting SOA_{243K→273K} particles exhibit higher overall apparent volatility,
 452 containing only 35% of LVOC/ELVOC/ULVOC (Figure S12 and Figure 6). Similarly, in the
 453 warming experiment from 273 K to 298 K, the fraction of LVOC/ELVOC/ULVOC decreased
 454 slightly from 16% to 15%, and from 18% to 14% in the case of SOA_{298K→313K} compared to
 455 SOA_{298K}. These results underscore the significant role of ambient temperature on the apparent
 456 volatility of SOA particles.



457
 458 Figure 6. Signal fraction of volatility groups (ULVOC, ELVOC, LVOC, SLVOC, IVOC, and VOC) in
 459 the SOA particles before (solid bars) and after (striped bars) warming process, respectively. Colors refer
 460 to the volatility groups. Volatility groups are identified based on the saturation concentrations as

461 described in the Method. Please note that the volatility groups in this Figure are related to their chamber
462 temperatures but not 298 K.

463 It should be noted that the FIGAERO-iodide-CIMS exhibits higher sensitivity toward moderate
464 oxygenated compounds (e.g., 2-9 oxygen atoms) (Riva et al., 2019), which may introduce bias
465 in the VBS. Nevertheless, comparisons of signal-weighted VBS distributions across different
466 experimental conditions remain indicative of the effects of temperature and warming on particle
467 volatility and the related chemical processes. Here, we note that the precursor concentrations
468 used in this study are substantially higher than typical atmospheric levels. While such
469 conditions are typical in chamber experiments to generate sufficient particle mass for
470 instrument detection and >10 hours aging by warming, they may influence the underlying
471 chemical processes. Specifically, elevated VOC and O₃ concentrations can enhance the rates of
472 bimolecular reactions, potentially favoring radical-radical recombination, accelerating
473 oligomer formation (Zhao et al., 2023), and increasing SOA yields relative to ambient
474 conditions. These conditions may also shift the partitioning of semi-volatile species toward the
475 particle phase. Consequently, the volatility distributions reported here likely represent an upper
476 bound of reactivity and should be interpreted with caution when extrapolating to atmospheric
477 conditions.

478 Please note, that other condensed-phase chemical reactions may play a role during warming
479 process as well, e.g., dimers may decompose due to their chemical instability (Pospisilova et
480 al., 2020; Surdu et al., 2024), and the formation and condensation of molecules such as
481 peroxyhemiacetal and aldol has been found to be reversible and temperature-dependent.
482 However, it requires further studies to address this question systematically.

483 Furthermore, the oxidation states (OS_C) of SOA particles after warming were lower than that
484 of the particles formed directly at these temperatures. As mentioned above, increasing
485 temperatures during warming facilitate the evaporation of more volatile compounds. This
486 results in the organic components remaining in the particles being generally less volatile and
487 higher oxidized corresponding to a higher oxidation state of bulk SOA as measured by the HR-
488 AMS.

489 However, it cannot compensate for the composition difference (e.g., due to autoxidation
490 (Bianchi et al., 2019)) between SOA_{243K} and SOA_{273K} caused by different reaction pathways
491 and product distributions at the different formation temperatures. For example, the saturation
492 concentrations of the same compounds in SOA_{243K→273K} and SOA_{273K} systems are the same
493 because they are both at 273 K. We compared the molecular chemical composition of
494 SOA_{243K→273K} and SOA_{273K} (Figure S13c and g). The C₁₁₋₂₀ products make up a higher signal
495 fraction in SOA_{243K→273K} (66%) compared to the corresponding compound groups in the
496 SOA_{273K} (43%), and vice versa for C₄₋₁₀ products. Higher mean OS_C values are found for
497 dimeric groups of C₁₃₋₁₅ as well as C₂₀, and other products of C₆ and C₁₆ in SOA_{273K}, leading to
498 higher OS_C for bulk SOA particles. Thus, we emphasize that, besides promoting the
499 condensation of condensable components, lower temperatures chemically enhance the
500 formation of ISO-AP cross dimers, while higher temperatures may favor the formation of higher
501 oxidized products, e.g., via the autoxidation mechanism (Bianchi et al., 2019).

502 For instance, SOA_{298K→313K} has OS_C values of -0.53 (HR-AMS) and -0.31 (FIGAERO-iodide-
503 CIMS), much lower than those of SOA_{313K} (-0.49 by HR-AMS and -0.27 by FIGAERO-iodide-
504 CIMS). By comparing the molecular chemical composition of both particles at 313 K (Figure

505 S13 a and e), the higher mean OS_C values for carbon groups of C₄₋₁₀ in SOA formed directly at
506 313 K cause the increase of overall OS_C of oxygenated products. This confirms again that higher
507 temperatures favour the formation of higher oxidized products.

508 In addition, C₈₋₁₀ compounds (mean formula C_{8.4}H_{12.4}O_{5.0}) in SOA_{298K→313K} have a T_{\max} of 100
509 °C. However, C₈₋₁₀ compounds have a similar mean formula (C_{8.5}H_{12.5}O_{5.3}) in SOA_{313K} but have
510 a lower T_{\max} of 82 °C. This implies that C₈₋₁₀ compounds consist of varying monomeric isomers
511 with significantly different volatilities, being less volatile in SOA_{298K→313K} and more volatile in
512 SOA_{313K}.

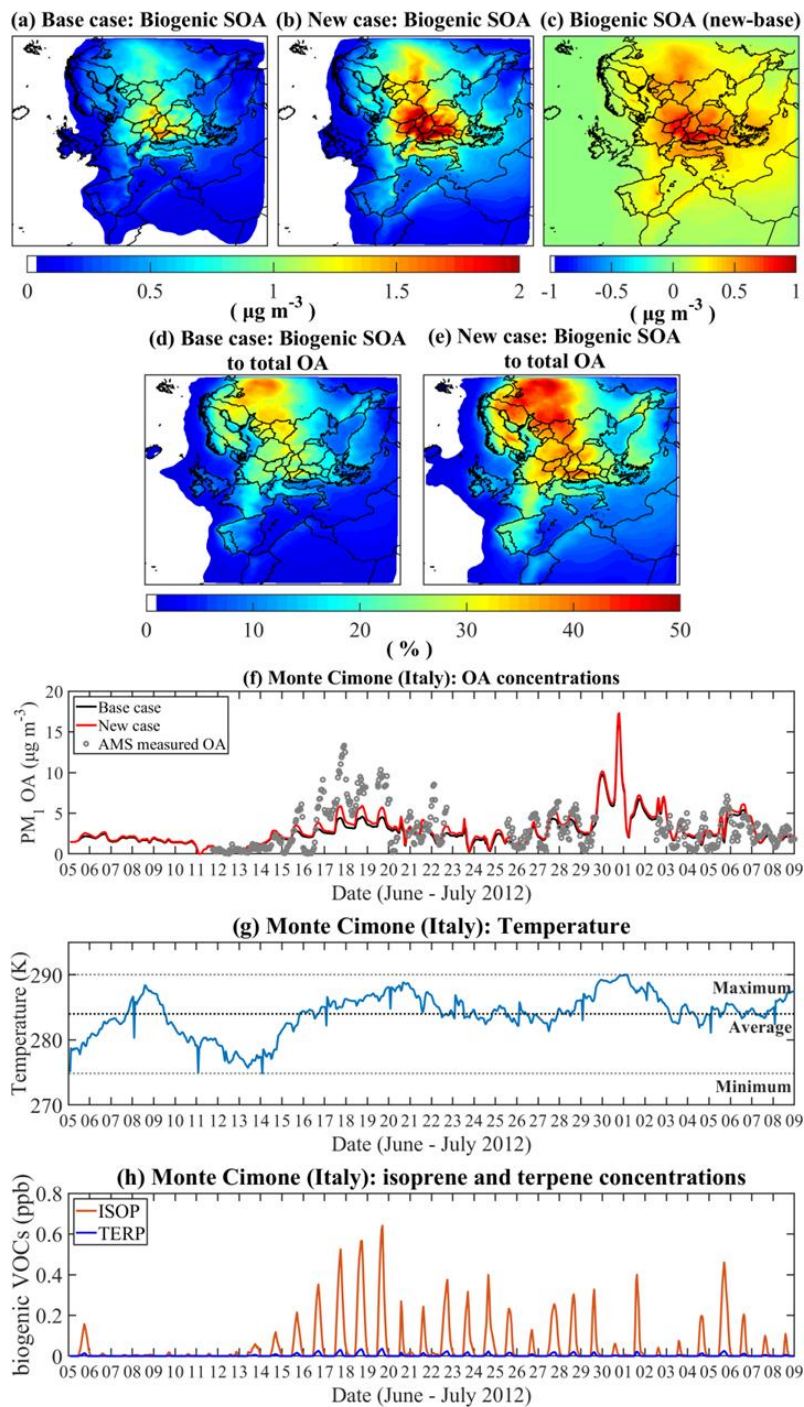
513 Besides, although SOA_{273K→298K} has the largest OS_C increment (-0.75 for bulk, -0.41 for
514 oxygenated constituents) from its initial particles before warming among all particles discussed,
515 its oxidation state is still significantly lower than SOA_{298K} (-0.56 for bulk, -0.31 for oxygenated
516 constituents). This is consistent with the somewhat higher volatility of SOA_{273K→298K} (T_{\max} of
517 71 °C) than SOA_{298K} (T_{\max} of 77 °C, Figure 5b and c) observed. All compound groups remaining
518 after warming have higher mean OS_C except for C₄ (Figure S13). This means that the
519 compounds in most compound groups are more oxidized when formed at 298 K. Thus, we
520 conclude that besides promoting the evaporation of particle-phase compounds, higher
521 temperatures also enhance the formation of higher oxidized products in SOA from oxidation of
522 α -pinene and isoprene mixtures.

523 **3.3 Modelling the impact of cross dimers for real world scenarios**

524 The relevance of these findings is corroborated by model simulations that incorporates the new
525 VBS parameterization derived below, including mixed dimers. The results discussed above are
526 based on experiments with equal initial amounts of α -pinene and isoprene. However, in the
527 natural atmosphere, the α -pinene to isoprene ratios can vary substantially for different
528 temperatures (seasons, day/night) and in different regions, e.g., boreal forest, tropical forest,
529 and temperate regions. The averaged ratio of isoprene to terpenes (including other monoterpene
530 compounds) over Europe during the simulation period is predicted to be 3.75 (Figure S3). With
531 α -pinene representing terpenes, simulations using the PMCAMx chemical transport model
532 (Tsimpidi et al., 2010; Fountoukis et al., 2011; Murphy and Pandis, 2009) show that when the
533 C₁₄₋₁₅ ISO-AP dimers are considered under different temperatures, the predicted mass
534 concentration of organics over Europe is significantly enhanced. The mean ground-level PM₁
535 biogenic SOA mass concentrations over Europe for the simulated period are found to increase
536 by 47% from 0.23 $\mu\text{g m}^{-3}$ with the original setup (Base case, Table S1) to 0.41 $\mu\text{g m}^{-3}$ by
537 utilizing the new VBS parameterization including the temperature dependent C₁₄₋₁₅ ISO-AP
538 cross dimers (New case, Table S2) (Figure 7a, b, c). The contribution of biogenic SOA to the
539 total OA mass increased from 9 to 14 % (Figure 7d, e). Specifically, in the New case, the
540 predicted ground-level OA mass concentrations are on average higher by 0.6 $\mu\text{g m}^{-3}$ for four
541 measuring stations located in Italy (Figure S4), as shown in Figure S14.

542 During the simulated period, the isoprene emissions are greater over Croatia than other
543 European areas. As a result, the difference in monthly averaged ground-level biogenic SOA
544 concentrations between the two simulations is larger in Croatia (0.9 $\mu\text{g m}^{-3}$) than the domain
545 average (0.4 $\mu\text{g m}^{-3}$). Figure S15 shows the correlation between isoprene concentrations and
546 the enhancement of biogenic SOA mass predicted in the New case compared to the Base case
547 over Croatia. In addition, due to the synergetic effect of relatively high concentrations of
548 biogenic precursors and higher temperatures (Figure 7g-h), the simulated biogenic SOA

549 concentrations at the site of Monte Cimone (2165 m.a.s.l.) show a better fit with the observed
 550 values compared to the Base case (Figure 7f).



551

552 Figure 7. The effect of the newly developed VBS parametrization on the predicted ground-level
 553 concentrations of biogenic SOA and total OA in PM₁ over Europe. Spatial distribution of the domain
 554 average biogenic SOA concentrations predicted utilizing (a) the original parametrization (Base case);
 555 (b) the new parameters derived considering the temperature dependent ISO-AP cross dimers (New case)
 556 and (c) the difference between the two simulations (New case – Base case); the contribution of the
 557 predicted biogenic SOA to the total OA concentrations over Europe in (d) the Base case and (e) the New
 558 case; (f) hourly ground-level OA concentrations predicted by the two simulations and measured by HR-
 559 AMS in the measuring site of Monte Cimone (Italy) during the PEGASUS campaign (June-July 2012);

560 (g) the simulated hourly temperature profile (1st simulation layer) and (h) the predicted isoprene (ISOP)
561 and terpene (TERP) ground-level concentrations over the measuring site for the simulated period.

562 **4. Conclusions**

563 This study utilized ¹³C-labeled isoprene to identify cross-dimeric products from parallel
564 oxidation of isoprene and α -pinene while examining SOA composition and volatility covering
565 most tropospheric conditions with temperatures between 213 K and 313 K. The identified C₁₄-
566 ₁₅ ISO-AP cross dimers suppress the formation of the α -pinene self-dimers (AP-AP). This is
567 achieved by competing with α -pinene-derived peroxy radicals (which are generated via OH-
568 oxidation), thereby inhibiting their reactions. This suppression effect is more pronounced at
569 lower temperatures between 213 – 273 K, while it is not temperature-sensitive above 273 K.
570 SOA components observed are more oxidized at higher temperatures which is consistent with
571 previous studies, potentially driven by a larger contribution from autoxidation pathways (Gao
572 et al., 2022; Bianchi et al., 2019; Ye et al., 2019). Warming experiments reveal significant
573 volatility changes: SOA formed at 243 K is and remains solid/semi-solid, losing only 18% of
574 particle-phase compounds upon warming to 273 K. In contrast, SOA formed at 273 K
575 undergoes substantial transition from a semi-solid to a liquid phase when being warmed to 298
576 K, losing 72.5% of all the particle-phase C_xH_yO_z compounds detected by FIGAERO-CIMS.
577 At 298 K, SOA shows lower O:C ratios and a 42% loss of oxygenated organics when warmed
578 to 313 K. Except for particles formed at 273 K and subsequently warmed to 298 K, in all other
579 temperature regimes, SOA formed directly at higher temperatures is both more oxidized and
580 more volatile than SOA formed at lower temperatures and then warmed. This observation has
581 implications for SOA evolution over diurnal cycles. For example, in mid-latitude or tropical
582 environments, SOA formed during warmer daytime hours may be more oxidized yet more
583 volatile to reversible evaporation. In contrast, SOA generated during cooler nighttime periods
584 would be less oxidized but more persistent, forming a low-volatility reservoir. This daily
585 alternation could significantly influence the overall lifetime, chemical aging, and mass yield of
586 SOA particles on a regional scale.

587 Implementing this new mechanistic and volatility information in the PMCAMx model resulted
588 in higher predicted SOA over Europe. Future studies should extend this modelling to a broader
589 ground-level temperature range and evaluate it with extensive field data. Furthermore, although
590 this study focuses on isoprene and α -pinene mixtures, other biogenic and anthropogenic VOC
591 mixtures may exhibit similar temperature-sensitive behaviour. Therefore, further studies are
592 warranted to elucidate the impact of temperature on SOA formation from diverse VOC mixtures,
593 which will extend our understanding and improve predictions in the context of a warming
594 climate.

595 **Data availability**

596 Data used in this manuscript are publicly available (KITopen data link once DOI is available).

597 **Acknowledgements**

598 This work was supported by H2020 European Research Council (CHAPAs (grant no. 850614)).
599 L.G., and J.S. acknowledge the China Scholarship Council (CSC) for financial support and the
600 Graduate School for Climate and Environment (GRACE). The authors thank the IMK-AAF
601 technicians at the KIT for their support of this work.

602 **Author contributions**

603 L.G and H.S designed the study. Chamber experiments were carried out by L.G, H.S, and J.S.
604 Data analysis and interpretation were performed by L.G, J.S., H.S, C.M, and C.W. Model
605 simulations and interpretation were done by S.E.I.M, S.N.P, L.G, and H.S. The manuscript was
606 written by L.G, with input from S.E.I.M, C.M, J.S, C.W, T.L, S.N.P, and H.S. All co-authors
607 commented on the manuscript.

608 **Competing interests**

609 The authors declare no competing financial interest. Please note, that at least one of the authors
610 is co-editor of ACP.

611

612 **References**

- 613 Andrae, M. O., Afchine, A., Albrecht, R., Holanda, B. A., Artaxo, P., Barbosa, H. M. J., Borrmann, S.,
614 Cecchini, M. A., Costa, A., Dollner, M., Fütterer, D., Järvinen, E., Jurkat, T., Klimach, T., Konemann, T.,
615 Knote, C., Krämer, M., Krisna, T., Machado, L. A. T., Mertes, S., Minikin, A., Pöhlker, C., Pöhlker, M. L.,
616 Pöschl, U., Rosenfeld, D., Sauer, D., Schlager, H., Schnaiter, M., Schneider, J., Schulz, C., Spanu, A.,
617 Sperling, V. B., Voigt, C., Walser, A., Wang, J., Weinzierl, B., Wendisch, M., and Ziereis, H.: Aerosol
618 characteristics and particle production in the upper troposphere over the Amazon Basin, *Atmos. Chem.*
619 *Phys.*, 18, 921-961, 10.5194/acp-18-921-2018, 2018.
- 620 Aubry, T. J., Staunton-Sykes, J., Marshall, L. R., Haywood, J., Abraham, N. L., and Schmidt, A.: Climate
621 change modulates the stratospheric volcanic sulfate aerosol lifecycle and radiative forcing from
622 tropical eruptions, *Nat. Commun.*, 12, 4708, 10.1038/s41467-021-24943-7, 2021.
- 623 Bernard, F., Fedioun, I., Peyroux, F., Quilgars, A., Daële, V., and Mellouki, A.: Thresholds of secondary
624 organic aerosol formation by ozonolysis of monoterpenes measured in a laminar flow aerosol reactor,
625 *J. Aerosol Sci.*, 43, 14-30, <https://doi.org/10.1016/j.jaerosci.2011.08.005>, 2012.
- 626 Bianchi, F., Kurtén, T., Riva, M., Mohr, C., Rissanen, M. P., Roldin, P., Berndt, T., Crouse, J. D.,
627 Wennberg, P. O., Mentel, T. F., Wildt, J., Junninen, H., Jokinen, T., Kulmala, M., Worsnop, D. R.,
628 Thornton, J. A., Donahue, N., Kjaergaard, H. G., and Ehn, M.: Highly Oxygenated Organic Molecules
629 (HOM) from Gas-Phase Autoxidation Involving Peroxy Radicals: A Key Contributor to Atmospheric
630 Aerosol, *Chemical Reviews*, 119, 3472-3509, 10.1021/acs.chemrev.8b00395, 2019.
- 631 Bilde, M., Barsanti, K., Booth, M., Cappa, C. D., Donahue, N. M., Emanuelsson, E. U., McFiggans, G.,
632 Krieger, U. K., Marcolli, C., Topping, D., Ziemann, P., Barley, M., Clegg, S., Dennis-Smith, B., Hallquist,
633 M., Hallquist, Å. M., Khlystov, A., Kulmala, M., Mogensen, D., Percival, C. J., Pope, F., Reid, J. P., Ribeiro
634 da Silva, M. A. V., Rosenoern, T., Salo, K., Soonsin, V. P., Yli-Juuti, T., Prisle, N. L., Pagels, J., Rarey, J.,
635 Zardini, A. A., and Riipinen, I.: Saturation Vapor Pressures and Transition Enthalpies of Low-Volatility
636 Organic Molecules of Atmospheric Relevance: From Dicarboxylic Acids to Complex Mixtures, *Chem.*
637 *Rev.*, 115, 4115-4156, 10.1021/cr5005502, 2015.
- 638 Campuzano-Jost, P., Williams, M. B., D'Ottone, L., and Hynes, A. J.: Kinetics and Mechanism of the
639 Reaction of the Hydroxyl Radical with h8-Isoprene and d8-Isoprene: Isoprene Absorption Cross
640 Sections, Rate Coefficients, and the Mechanism of Hydroperoxyl Radical Production, *The Journal of*
641 *Physical Chemistry A*, 108, 1537-1551, 10.1021/jp0363601, 2004.
- 642 Campuzano-Jost, P., Williams, M. B., O'Otton, L., and Hynes, A. J.: Kinetics of the OH-initiated
643 oxidation of isoprene, *Geophysical Research Letters*, 27, 693-696,
644 <https://doi.org/10.1029/1999GL010995>, 2000.
- 645 Carlton, A. G., Wiedinmyer, C., and Kroll, J. H.: A review of Secondary Organic Aerosol (SOA) formation
646 from isoprene, *Atmos. Chem. Phys.*, 9, 4987-5005, 10.5194/acp-9-4987-2009, 2009.
- 647 Curtius, J., Heinritzi, M., Beck, L. J., Pöhlker, M. L., Tripathi, N., Krumm, B. E., Holzbeck, P., Nussbaumer,
648 C. M., Hernández Pardo, L., Klimach, T., Barmounis, K., Andersen, S. T., Bardakov, R., Bohn, B., Cecchini,
649 M. A., Chaboureau, J.-P., Dauhut, T., Dienhart, D., Dörich, R., Edtbauer, A., Giez, A., Hartmann, A.,
650 Holanda, B. A., Joppe, P., Kaiser, K., Keber, T., Klebach, H., Krüger, O. O., Kürten, A., Mallaun, C., Marno,
651 D., Martinez, M., Monteiro, C., Nelson, C., Ort, L., Raj, S. S., Richter, S., Ringsdorf, A., Rocha, F., Simon,
652 M., Sreekumar, S., Tsokankunku, A., Unfer, G. R., Valenti, I. D., Wang, N., Zahn, A., Zauner-Wieczorek,
653 M., Albrecht, R. I., Andrae, M. O., Artaxo, P., Crowley, J. N., Fischer, H., Harder, H., Herdies, D. L.,
654 Machado, L. A. T., Pöhlker, C., Pöschl, U., Possner, A., Pozzer, A., Schneider, J., Williams, J., and Lelieveld,
655 J.: Isoprene nitrates drive new particle formation in Amazon's upper troposphere, *Nature*, 636, 124-
656 130, 10.1038/s41586-024-08192-4, 2024.
- 657 DeRieux, W. S. W., Li, Y., Lin, P., Laskin, J., Laskin, A., Bertram, A. K., Nizkorodov, S. A., and Shiraiwa, M.:
658 Predicting the glass transition temperature and viscosity of secondary organic material using molecular
659 composition, *Atmos. Chem. Phys.*, 18, 6331-6351, 10.5194/acp-18-6331-2018, 2018.
- 660 Dillon, T. J., Dulitz, K., Groß, C. B. M., and Crowley, J. N.: Temperature-dependent rate coefficients for
661 the reactions of the hydroxyl radical with the atmospheric biogenics isoprene, alpha-pinene and delta-
662 3-carene, *Atmos. Chem. Phys.*, 17, 15137-15150, 10.5194/acp-17-15137-2017, 2017.

663 Donahue, N. M., Robinson, A. L., Stanier, C. O., and Pandis, S. N.: Coupled Partitioning, Dilution, and
664 Chemical Aging of Semivolatile Organics, *Environ. Sci. Technol.*, 40, 2635-2643, 10.1021/es052297c,
665 2006.

666 Fountoukis, C., Racherla, P. N., Denier van der Gon, H. A. C., Polymeneas, P., Charalampidis, P. E., Pilinis,
667 C., Wiedensohler, A., Dall'Osto, M., O'Dowd, C., and Pandis, S. N.: Evaluation of a three-dimensional
668 chemical transport model (PMCAMx) in the European domain during the EUCAARI May 2008 campaign,
669 *Atmos. Chem. Phys.*, 11, 10331-10347, 10.5194/acp-11-10331-2011, 2011.

670 Fu, P., Kawamura, K., Chen, J., and Barrie, L. A.: Isoprene, Monoterpene, and Sesquiterpene Oxidation
671 Products in the High Arctic Aerosols during Late Winter to Early Summer, *Environ. Sci. Technol.*, 43,
672 4022-4028, 10.1021/es803669a, 2009.

673 Gao, L., Song, J., Mohr, C., Huang, W., Vallon, M., Jiang, F., Leisner, T., and Saathoff, H.: Kinetics, SOA
674 yields, and chemical composition of secondary organic aerosol from β -caryophyllene ozonolysis with
675 and without nitrogen oxides between 213 and 313 K, *Atmos. Chem. Phys.*, 22, 6001-6020,
676 10.5194/acp-22-6001-2022, 2022.

677 Gao, L., Buchholz, A., Li, Z., Song, J., Vallon, M., Jiang, F., Möhler, O., Leisner, T., and Saathoff, H.:
678 Volatility of Secondary Organic Aerosol from β -Caryophyllene Ozonolysis over a Wide Tropospheric
679 Temperature Range, *Environmental Science & Technology*, 57, 8965-8974, 10.1021/acs.est.3c01151,
680 2023.

681 Gkatzelis, G. I., Hohaus, T., Tillmann, R., Gensch, I., Müller, M., Eichler, P., Xu, K. M., Schlag, P., Schmitt,
682 S. H., Yu, Z., Wegener, R., Kaminski, M., Holzinger, R., Wisthaler, A., and Kiendler-Scharr, A.: Gas-to-
683 particle partitioning of major biogenic oxidation products: a study on freshly formed and aged biogenic
684 SOA, *Atmos. Chem. Phys.*, 18, 12969-12989, 10.5194/acp-18-12969-2018, 2018.

685 Guenther, A., Karl, T., Harley, P., Wiedinmyer, C., Palmer, P. I., and Geron, C.: Estimates of global
686 terrestrial isoprene emissions using MEGAN (Model of Emissions of Gases and Aerosols from Nature),
687 *Atmos. Chem. Phys.*, 6, 3181-3210, 10.5194/acp-6-3181-2006, 2006.

688 Hallquist, M., Wenger, J. C., Baltensperger, U., Rudich, Y., Simpson, D., Claeys, M., Dommen, J.,
689 Donahue, N. M., George, C., Goldstein, A. H., Hamilton, J. F., Herrmann, H., Hoffmann, T., Iinuma, Y.,
690 Jang, M., Jenkin, M. E., Jimenez, J. L., Kiendler-Scharr, A., Maenhaut, W., McFiggans, G., Mentel, T. F.,
691 Monod, A., Prévôt, A. S. H., Seinfeld, J. H., Surratt, J. D., Szmigielski, R., and Wildt, J.: The formation,
692 properties and impact of secondary organic aerosol: current and emerging issues, *Atmos. Chem. Phys.*,
693 9, 5155-5236, 10.5194/acp-9-5155-2009, 2009.

694 Hansen, J., Sato, M., Ruedy, R., Lo, K., Lea, D. W., and Medina-Elizade, M.: Global temperature change,
695 *Proc. Natl. Acad. Sci.*, 103, 14288-14293, doi:10.1073/pnas.0606291103, 2006.

696 Heald, C. L., Kroll, J. H., Jimenez, J. L., Docherty, K. S., DeCarlo, P. F., Aiken, A. C., Chen, Q., Martin, S. T.,
697 Farmer, D. K., and Artaxo, P.: A simplified description of the evolution of organic aerosol composition
698 in the atmosphere, *Geophysical Research Letters*, 37, <https://doi.org/10.1029/2010GL042737>, 2010.

699 Heinritzi, M., Dada, L., Simon, M., Stolzenburg, D., Wagner, A. C., Fischer, L., Ahonen, L. R., Amanatidis,
700 S., Baalbaki, R., Baccarini, A., Bauer, P. S., Baumgartner, B., Bianchi, F., Brilke, S., Chen, D., Chiu, R., Dias,
701 A., Dommen, J., Duplissy, J., Finkenzeller, H., Frege, C., Fuchs, C., Garmash, O., Gordon, H., Granzin, M.,
702 El Haddad, I., He, X., Helm, J., Hofbauer, V., Hoyle, C. R., Kangasluoma, J., Keber, T., Kim, C., Kürten, A.,
703 Lamkaddam, H., Laurila, T. M., Lampilahti, J., Lee, C. P., Lehtipalo, K., Leiminger, M., Mai, H.,
704 Makhmutov, V., Manninen, H. E., Marten, R., Mathot, S., Mauldin, R. L., Mentler, B., Molteni, U., Müller,
705 T., Nie, W., Nieminen, T., Onnela, A., Partoll, E., Passananti, M., Petäjä, T., Pfeifer, J., Pospisilova, V.,
706 Quéléver, L. L. J., Rissanen, M. P., Rose, C., Schobesberger, S., Scholz, W., Scholze, K., Sipilä, M., Steiner,
707 G., Stozhkov, Y., Tauber, C., Tham, Y. J., Vazquez-Pufleau, M., Virtanen, A., Vogel, A. L., Volkamer, R.,
708 Wagner, R., Wang, M., Weitz, L., Wimmer, D., Xiao, M., Yan, C., Ye, P., Zha, Q., Zhou, X., Amorim, A.,
709 Baltensperger, U., Hansel, A., Kulmala, M., Tomé, A., Winkler, P. M., Worsnop, D. R., Donahue, N. M.,
710 Kirkby, J., and Curtius, J.: Molecular understanding of the suppression of new-particle formation by
711 isoprene, *Atmos. Chem. Phys.*, 20, 11809-11821, 10.5194/acp-20-11809-2020, 2020.

712 Jimenez, J. L., Canagaratna, M. R., Donahue, N. M., Prevot, A. S. H., Zhang, Q., Kroll, J. H., DeCarlo, P.
713 F., Allan, J. D., Coe, H., Ng, N. L., Aiken, A. C., Docherty, K. S., Ulbrich, I. M., Grieshop, A. P., Robinson,

714 A. L., Duplissy, J., Smith, J. D., Wilson, K. R., Lanz, V. A., Hueglin, C., Sun, Y. L., Tian, J., Laaksonen, A.,
715 Raatikainen, T., Rautiainen, J., Vaattovaara, P., Ehn, M., Kulmala, M., Tomlinson, J. M., Collins, D. R.,
716 Cubison, M. J., E., Dunlea, J., Huffman, J. A., Onasch, T. B., Alfarra, M. R., Williams, P. I., Bower, K.,
717 Kondo, Y., Schneider, J., Drewnick, F., Borrmann, S., Weimer, S., Demerjian, K., Salcedo, D., Cottrell, L.,
718 Griffin, R., Takami, A., Miyoshi, T., Hatakeyama, S., Shimono, A., Sun, J. Y., Zhang, Y. M., Dzepina, K.,
719 Kimmel, J. R., Sueper, D., Jayne, J. T., Herndon, S. C., Trimborn, A. M., Williams, L. R., Wood, E. C.,
720 Middlebrook, A. M., Kolb, C. E., Baltensperger, U., and Worsnop, D. R.: Evolution of Organic Aerosols
721 in the Atmosphere, *Science*, 326, 1525-1529, doi:10.1126/science.1180353, 2009.

722 Jonsson, Å. M., Hallquist, M., and Ljungström, E.: The effect of temperature and water on secondary
723 organic aerosol formation from ozonolysis of limonene, Δ^3 -carene and α -pinene,
724 *Atmos. Chem. Phys.*, 8, 6541-6549, 10.5194/acp-8-6541-2008, 2008.

725 Kanakidou, M., Seinfeld, J. H., Pandis, S. N., Barnes, I., Dentener, F. J., Facchini, M. C., Van Dingenen,
726 R., Ervens, B., Nenes, A., Nielsen, C. J., Swietlicki, E., Putaud, J. P., Balkanski, Y., Fuzzi, S., Horth, J.,
727 Moortgat, G. K., Winterhalter, R., Myhre, C. E. L., Tsigaridis, K., Vignati, E., Stephanou, E. G., and Wilson,
728 J.: Organic aerosol and global climate modelling: a review, *Atmos. Chem. Phys.*, 5, 1053-1123,
729 10.5194/acp-5-1053-2005, 2005.

730 Khamaganov, V. G. and Hites, R. A.: Rate Constants for the Gas-Phase Reactions of Ozone with Isoprene,
731 α - and β -Pinene, and Limonene as a Function of Temperature, *J. Phys. Chem. A*, 105, 815-822,
732 10.1021/jp002730z, 2001.

733 Kiendler-Scharr, A., Wildt, J., Maso, M. D., Hohaus, T., Kleist, E., Mentel, T. F., Tillmann, R., Uerlings, R.,
734 Schurr, U., and Wahner, A.: New particle formation in forests inhibited by isoprene emissions, *Nature*,
735 461, 381-384, 10.1038/nature08292, 2009.

736 Kourtchev, I., Doussin, J. F., Giorio, C., Mahon, B., Wilson, E. M., Maurin, N., Pangu, E., Venables, D. S.,
737 Wenger, J. C., and Kalberer, M.: Molecular composition of fresh and aged secondary organic aerosol
738 from a mixture of biogenic volatile compounds: a high-resolution mass spectrometry study, *Atmos.*
739 *Chem. Phys.*, 15, 5683-5695, 10.5194/acp-15-5683-2015, 2015.

740 Kroll, J. H. and Seinfeld, J. H.: Chemistry of secondary organic aerosol: Formation and evolution of low-
741 volatility organics in the atmosphere, *Atmos. Environ.*, 42, 3593-3624,
742 <https://doi.org/10.1016/j.atmosenv.2008.01.003>, 2008.

743 Ladino, L. A., Zhou, S., Yakobi-Hancock, J. D., Aljawhary, D., and Abbatt, J. P. D.: Factors controlling the
744 ice nucleating abilities of α -pinene SOA particles, *J. Geophys. Res.*, 119, 9041-9051,
745 <https://doi.org/10.1002/2014JD021578>, 2014.

746 Lamb, R. C., Pacifici, J. G., and Ayers, P. W.: Organic Peroxides. IV. Kinetics and Products of
747 Decompositions of Cyclohexaneformyl and Isobutyryl Peroxides. BDPA as a Free-Radical Scavenger¹, *J.*
748 *Am. Chem. Soc.*, 87, 3928-3935, 10.1021/ja01095a024, 1965.

749 Lamkaddam, H., Dommen, J., Ranjithkumar, A., Gordon, H., Wehrle, G., Krechmer, J., Majluf, F.,
750 Salionov, D., Schmale, J., Bjelić, S., Carslaw, K. S., El Haddad, I., and Baltensperger, U.: Large
751 contribution to secondary organic aerosol from isoprene cloud chemistry, *Sci. Adv.*, 7, eabe2952,
752 doi:10.1126/sciadv.abe2952, 2021.

753 Lane, T. E., Donahue, N. M., and Pandis, S. N.: Simulating secondary organic aerosol formation using
754 the volatility basis-set approach in a chemical transport model, *Atmospheric Environment*, 42, 7439-
755 7451, <https://doi.org/10.1016/j.atmosenv.2008.06.026>, 2008.

756 Lee, B. H., Lopez-Hilfiker, F. D., Mohr, C., Kurtén, T., Worsnop, D. R., and Thornton, J. A.: An Iodide-
757 Adduct High-Resolution Time-of-Flight Chemical-Ionization Mass Spectrometer: Application to
758 Atmospheric Inorganic and Organic Compounds, *Environmental Science & Technology*, 48, 6309-6317,
759 10.1021/es500362a, 2014.

760 Leffler, J. E. and More, A. A.: Decomposition of bicyclo[2.2.2]-1-formyl and pivaloyl peroxides, *J. Am.*
761 *Chem. Soc.*, 94, 2483-2487, 10.1021/ja00762a048, 1972.

762 Li, H., Canagaratna, M. R., Riva, M., Rantala, P., Zhang, Y., Thomas, S., Heikkinen, L., Flaud, P. M.,
763 Villenave, E., Perraudin, E., Worsnop, D., Kulmala, M., Ehn, M., and Bianchi, F.: Atmospheric organic
764 vapors in two European pine forests measured by a Vocus PTR-TOF: insights into monoterpene and

765 sesquiterpene oxidation processes, *Atmos. Chem. Phys.*, 21, 4123-4147, 10.5194/acp-21-4123-2021,
766 2021.

767 Li, Y., Pöschl, U., and Shiraiwa, M.: Molecular corridors and parameterizations of volatility in the
768 chemical evolution of organic aerosols, *Atmos. Chem. Phys.*, 16, 3327-3344, 10.5194/acp-16-3327-
769 2016, 2016.

770 Liu, Y., Su, H., Wang, S., Wei, C., Tao, W., Pöhlker, M. L., Pöhlker, C., Holanda, B. A., Krüger, O. O.,
771 Hoffmann, T., Wendisch, M., Artaxo, P., Pöschl, U., Andreae, M. O., and Cheng, Y.: Strong particle
772 production and condensational growth in the upper troposphere sustained by biogenic VOCs from the
773 canopy of the Amazon Basin, *Atmos. Chem. Phys.*, 23, 251-272, 10.5194/acp-23-251-2023, 2023.

774 Lopez-Hilfiker, F. D., Iyer, S., Mohr, C., Lee, B. H., D'Ambro, E. L., Kurtén, T., and Thornton, J. A.:
775 Constraining the sensitivity of iodide adduct chemical ionization mass spectrometry to multifunctional
776 organic molecules using the collision limit and thermodynamic stability of iodide ion adducts, *Atmos.*
777 *Meas. Tech.*, 9, 1505-1512, 10.5194/amt-9-1505-2016, 2016.

778 Lopez-Hilfiker, F. D., Mohr, C., Ehn, M., Rubach, F., Kleist, E., Wildt, J., Mentel, T. F., Lutz, A., Hallquist,
779 M., Worsnop, D., and Thornton, J. A.: A novel method for online analysis of gas and particle
780 composition: description and evaluation of a Filter Inlet for Gases and AEROSols (FIGAERO), *Atmos.*
781 *Meas. Tech.*, 7, 983-1001, 10.5194/amt-7-983-2014, 2014.

782 Lopez-Hilfiker, F. D., Mohr, C., Ehn, M., Rubach, F., Kleist, E., Wildt, J., Mentel, T. F., Carrasquillo, A. J.,
783 Daumit, K. E., Hunter, J. F., Kroll, J. H., Worsnop, D. R., and Thornton, J. A.: Phase partitioning and
784 volatility of secondary organic aerosol components formed from α -pinene ozonolysis and OH oxidation:
785 the importance of accretion products and other low volatility compounds, *Atmos. Chem. Phys.*, 15,
786 7765-7776, 10.5194/acp-15-7765-2015, 2015.

787 Mahowald, N.: Aerosol Indirect Effect on Biogeochemical Cycles and Climate, *Science*, 334, 794-796,
788 doi:10.1126/science.1207374, 2011.

789 Manavi, S. E. I. and Pandis, S. N.: A lumped species approach for the simulation of secondary organic
790 aerosol production from intermediate-volatility organic compounds (IVOCs): application to road
791 transport in PMCAMx-iv (v1.0), *Geosci. Model Dev.*, 15, 7731-7749, 10.5194/gmd-15-7731-2022, 2022.

792 Manavi, S. E. I. and Pandis, S. N.: Contribution of intermediate-volatility organic compounds from on-
793 road transport to secondary organic aerosol levels in Europe, *Atmos. Chem. Phys.*, 24, 891-909,
794 10.5194/acp-24-891-2024, 2024.

795 McFiggans, G., Mentel, T. F., Wildt, J., Pullinen, I., Kang, S., Kleist, E., Schmitt, S., Springer, M., Tillmann,
796 R., Wu, C., Zhao, D., Hallquist, M., Faxon, C., Le Breton, M., Hallquist, Å. M., Simpson, D., Bergström,
797 R., Jenkin, M. E., Ehn, M., Thornton, J. A., Alfarra, M. R., Bannan, T. J., Percival, C. J., Priestley, M.,
798 Topping, D., and Kiendler-Scharr, A.: Secondary organic aerosol reduced by mixture of atmospheric
799 vapours, *Nature*, 565, 587-593, 10.1038/s41586-018-0871-y, 2019.

800 Möhler, O., Stetzer, O., Schaefers, S., Linke, C., Schnaiter, M., Tiede, R., Saathoff, H., Krämer, M.,
801 Mangold, A., Budz, P., Zink, P., Schreiner, J., Mauersberger, K., Haag, W., Kärcher, B., and Schurath, U.:
802 Experimental investigation of homogeneous freezing of sulphuric acid particles in the aerosol chamber
803 AIDA, *Atmos. Chem. Phys.*, 3, 211-223, 10.5194/acp-3-211-2003, 2003.

804 Morino, Y., Sato, K., Jathar, S. H., Tanabe, K., Inomata, S., Fujitani, Y., Ramasamy, S., and Cappa, C. D.:
805 Modeling the Effects of Dimerization and Bulk Diffusion on the Evaporative Behavior of Secondary
806 Organic Aerosol Formed from α -Pinene and 1,3,5-Trimethylbenzene, *ACS Earth Space Chem.*, 4, 1931-
807 1946, 10.1021/acsearthspacechem.0c00106, 2020.

808 Murphy, B. N. and Pandis, S. N.: Simulating the Formation of Semivolatile Primary and Secondary
809 Organic Aerosol in a Regional Chemical Transport Model, *Environmental Science & Technology*, 43,
810 4722-4728, 10.1021/es803168a, 2009.

811 Owen, S. M., MacKenzie, A. R., Stewart, H., Donovan, R., and Hewitt, C. N.: BIOGENIC VOLATILE
812 ORGANIC COMPOUND (VOC) EMISSION ESTIMATES FROM AN URBAN TREE CANOPY, *Ecol. Appl.*, 13,
813 927-938, <https://doi.org/10.1890/01-5177>, 2003.

814 Paasonen, P., Asmi, A., Petäjä, T., Kajos, M. K., Äijälä, M., Junninen, H., Holst, T., Abbatt, J. P. D., Arneth,
815 A., Birmili, W., van der Gon, H. D., Hamed, A., Hoffer, A., Laakso, L., Laaksonen, A., Richard Leaitch, W.,

816 Plass-Dülmer, C., Pryor, S. C., Räisänen, P., Swietlicki, E., Wiedensohler, A., Worsnop, D. R., Kerminen,
817 V.-M., and Kulmala, M.: Warming-induced increase in aerosol number concentration likely to
818 moderate climate change, *Nat. Geosci.*, 6, 438-442, 10.1038/ngeo1800, 2013.

819 Pajunoja, A., Lambe, A. T., Hakala, J., Rastak, N., Cummings, M. J., Brogan, J. F., Hao, L., Paramonov, M.,
820 Hong, J., Prisle, N. L., Malila, J., Romakkaniemi, S., Lehtinen, K. E. J., Laaksonen, A., Kulmala, M., Massoli,
821 P., Onasch, T. B., Donahue, N. M., Riipinen, I., Davidovits, P., Worsnop, D. R., Petäjä, T., and Virtanen,
822 A.: Adsorptive uptake of water by semisolid secondary organic aerosols, *Geophys. Res. Lett.*, 42, 3063-
823 3068, <https://doi.org/10.1002/2015GL063142>, 2015.

824 Petersen, R., Holst, T., Mölder, M., Kljun, N., and Rinne, J.: Vertical distribution of sources and sinks of
825 volatile organic compounds within a boreal forest canopy, *Atmos. Chem. Phys.*, 23, 7839-7858,
826 10.5194/acp-23-7839-2023, 2023.

827 Pospisilova, V., Lopez-Hilfiker, F. D., Bell, D. M., El Haddad, I., Mohr, C., Huang, W., Heikkinen, L., Xiao,
828 M., Dommen, J., Prevot, A. S. H., Baltensperger, U., and Slowik, J. G.: On the fate of oxygenated organic
829 molecules in atmospheric aerosol particles, *Science Advances*, 6, eaax8922,
830 doi:10.1126/sciadv.aax8922, 2020.

831 Quéléver, L. L. J., Kristensen, K., Normann Jensen, L., Rosati, B., Teiwes, R., Daellenbach, K. R., Peräkylä,
832 O., Roldin, P., Bossi, R., Pedersen, H. B., Glasius, M., Bilde, M., and Ehn, M.: Effect of temperature on
833 the formation of highly oxygenated organic molecules (HOMs) from α -pinene ozonolysis, *Atmos. Chem.*
834 *Phys.*, 19, 7609-7625, 10.5194/acp-19-7609-2019, 2019.

835 Riva, M., Rantala, P., Krechmer, J. E., Peräkylä, O., Zhang, Y., Heikkinen, L., Garmash, O., Yan, C., Kulmala,
836 M., Worsnop, D., and Ehn, M.: Evaluating the performance of five different chemical ionization
837 techniques for detecting gaseous oxygenated organic species, *Atmos. Meas. Tech.*, 12, 2403-2421,
838 10.5194/amt-12-2403-2019, 2019.

839 Saathoff, H., Naumann, K. H., Möhler, O., Jonsson, Å. M., Hallquist, M., Kiendler-Scharr, A., Mentel, T.
840 F., Tillmann, R., and Schurath, U.: Temperature dependence of yields of secondary organic aerosols
841 from the ozonolysis of α -pinene and limonene, *Atmos. Chem. Phys.*, 9, 1551-1577, 10.5194/acp-9-
842 1551-2009, 2009.

843 Schilling Fahnstock, K. A., Yee, L. D., Loza, C. L., Coggon, M. M., Schwantes, R., Zhang, X., Dalleska, N.
844 F., and Seinfeld, J. H.: Secondary Organic Aerosol Composition from C12 Alkanes, *The Journal of*
845 *Physical Chemistry A*, 119, 4281-4297, 10.1021/jp501779w, 2015.

846 Schulz, C., Schneider, J., Amorim Holanda, B., Appel, O., Costa, A., de Sá, S. S., Dreiling, V., Fütterer, D.,
847 Jurkat-Witschas, T., Klimach, T., Knote, C., Krämer, M., Martin, S. T., Mertes, S., Pöhlker, M. L., Sauer,
848 D., Voigt, C., Walser, A., Weinzierl, B., Ziereis, H., Zöger, M., Andreae, M. O., Artaxo, P., Machado, L. A.
849 T., Pöschl, U., Wendisch, M., and Borrmann, S.: Aircraft-based observations of isoprene-epoxydiol-
850 derived secondary organic aerosol (IEPOX-SOA) in the tropical upper troposphere over the Amazon
851 region, *Atmos. Chem. Phys.*, 18, 14979-15001, 10.5194/acp-18-14979-2018, 2018.

852 Sheehan, P. E. and Bowman, F. M.: Estimated Effects of Temperature on Secondary Organic Aerosol
853 Concentrations, *Environ. Sci. Technol.*, 35, 2129-2135, 10.1021/es001547g, 2001.

854 Shiraiwa, M., Ammann, M., Koop, T., and Pöschl, U.: Gas uptake and chemical aging of semisolid
855 organic aerosol particles, *Proc. Natl. Acad. Sci.*, 108, 11003-11008, doi:10.1073/pnas.1103045108,
856 2011.

857 Shiraiwa, M., Li, Y., Tsimpidi, A. P., Karydis, V. A., Berkemeier, T., Pandis, S. N., Lelieveld, J., Koop, T.,
858 and Pöschl, U.: Global distribution of particle phase state in atmospheric secondary organic aerosols,
859 *Nat. Commun.*, 8, 15002, 10.1038/ncomms15002, 2017.

860 Simon, M., Dada, L., Heinritzi, M., Scholz, W., Stolzenburg, D., Fischer, L., Wagner, A. C., Kürten, A.,
861 Rörup, B., He, X. C., Almeida, J., Baalbaki, R., Baccharini, A., Bauer, P. S., Beck, L., Bergen, A., Bianchi, F.,
862 Bräkling, S., Brilke, S., Caudillo, L., Chen, D., Chu, B., Dias, A., Draper, D. C., Duplissy, J., El-Haddad, I.,
863 Finkenzeller, H., Frege, C., Gonzalez-Carracedo, L., Gordon, H., Granzin, M., Hakala, J., Hofbauer, V.,
864 Hoyle, C. R., Kim, C., Kong, W., Lamkaddam, H., Lee, C. P., Lehtipalo, K., Leiminger, M., Mai, H.,
865 Manninen, H. E., Marie, G., Marten, R., Mentler, B., Molteni, U., Nichman, L., Nie, W., Ojdanic, A.,
866 Onnela, A., Partoll, E., Petäjä, T., Pfeifer, J., Philippov, M., Quéléver, L. L. J., Ranjithkumar, A., Rissanen,

867 M. P., Schallhart, S., Schobesberger, S., Schuchmann, S., Shen, J., Sipilä, M., Steiner, G., Stozhkov, Y.,
868 Tauber, C., Tham, Y. J., Tomé, A. R., Vazquez-Pufleau, M., Vogel, A. L., Wagner, R., Wang, M., Wang, D.
869 S., Wang, Y., Weber, S. K., Wu, Y., Xiao, M., Yan, C., Ye, P., Ye, Q., Zauner-Wieczorek, M., Zhou, X.,
870 Baltensperger, U., Dommen, J., Flagan, R. C., Hansel, A., Kulmala, M., Volkamer, R., Winkler, P. M.,
871 Worsnop, D. R., Donahue, N. M., Kirkby, J., and Curtius, J.: Molecular understanding of new-particle
872 formation from α -pinene between -50 and $+25$ °C, *Atmos. Chem. Phys.*, 20, 9183-9207, 10.5194/acp-
873 20-9183-2020, 2020.

874 Sindelarova, K., Granier, C., Bouarar, I., Guenther, A., Tilmes, S., Stavrakou, T., Müller, J. F., Kuhn, U.,
875 Stefani, P., and Knorr, W.: Global data set of biogenic VOC emissions calculated by the MEGAN model
876 over the last 30 years, *Atmos. Chem. Phys.*, 14, 9317-9341, 10.5194/acp-14-9317-2014, 2014.

877 Sofiev, M., Vankevich, R., Lanne, M., Koskinen, J., and Kukkonen, J.: On Integration Of A Fire
878 Assimilation System And A Chemical Transport Model For Near-realtime Monitoring Of The Impact Of
879 Wild-land Fires On Atmospheric Composition And Air Quality, *WIT Trans. Ecol. Environ.*, 119, 343-351,
880 2008.

881 Stark, H., Yatavelli, R. L. N., Thompson, S. L., Kang, H., Krechmer, J. E., Kimmel, J. R., Palm, B. B., Hu, W.,
882 Hayes, P. L., Day, D. A., Campuzano-Jost, P., Canagaratna, M. R., Jayne, J. T., Worsnop, D. R., and
883 Jimenez, J. L.: Impact of Thermal Decomposition on Thermal Desorption Instruments: Advantage of
884 Thermogram Analysis for Quantifying Volatility Distributions of Organic Species, *Environmental
885 Science & Technology*, 51, 8491-8500, 10.1021/acs.est.7b00160, 2017.

886 Surdu, M., Top, J., Yang, B., Zhang, J., Slowik, J. G., Prévôt, A. S. H., Wang, D. S., el Haddad, I., and Bell,
887 D. M.: Real-Time Identification of Aerosol-Phase Carboxylic Acid Production Using Extractive
888 Electrospray Ionization Mass Spectrometry, *Environmental Science & Technology*, 58, 8857-8866,
889 10.1021/acs.est.4c01605, 2024.

890 Takeuchi, M., Berkemeier, T., Eris, G., and Ng, N. L.: Non-linear effects of secondary organic aerosol
891 formation and properties in multi-precursor systems, *Nat. Commun.*, 13, 7883, 10.1038/s41467-022-
892 35546-1, 2022.

893 Tripathi, N., Krumm, B. E., Edtbauer, A., Ringsdorf, A., Wang, N., Kohl, M., Vella, R., Machado, L. A. T.,
894 Pozzer, A., Lelieveld, J., and Williams, J.: Impacts of convection, chemistry, and forest clearing on
895 biogenic volatile organic compounds over the Amazon, *Nature Communications*, 16, 4692,
896 10.1038/s41467-025-59953-2, 2025.

897 Trump, E. R. and Donahue, N. M.: Oligomer formation within secondary organic aerosols: equilibrium
898 and dynamic considerations, *Atmos. Chem. Phys.*, 14, 3691-3701, 10.5194/acp-14-3691-2014, 2014.

899 Tsimpidi, A. P., Karydis, V. A., Zavala, M., Lei, W., Molina, L., Ulbrich, I. M., Jimenez, J. L., and Pandis, S.
900 N.: Evaluation of the volatility basis-set approach for the simulation of organic aerosol formation in the
901 Mexico City metropolitan area, *Atmos. Chem. Phys.*, 10, 525-546, 10.5194/acp-10-525-2010, 2010.

902 Vallon, M., Gao, L., Jiang, F., Krumm, B., Nadolny, J., Song, J., Leisner, T., and Saathoff, H.: LED-based
903 solar simulator to study photochemistry over a wide temperature range in the large simulation
904 chamber AIDA, *Atmos. Meas. Tech.*, 15, 1795-1810, 10.5194/amt-15-1795-2022, 2022.

905 Visschedijk, A., Zandveld, P., and Denier Van Der Gon, H.: A high resolution gridded European emission
906 database for the EU integrated project GEMS, TNO report, 2007.

907 Wagner, R., Bunz, H., Linke, C., Möhler, O., Naumann, K.-H., Saathoff, H., Schnaiter, M., and Schurath,
908 U.: Chamber Simulations of Cloud Chemistry: The AIDA Chamber, *Environmental Simulation Chambers:
909 Application to Atmospheric Chemical Processes*, Dordrecht, 2006//, 67-82,

910 Wang, Y., Zhao, Y., Li, Z., Li, C., Yan, N., and Xiao, H.: Importance of Hydroxyl Radical Chemistry in
911 Isoprene Suppression of Particle Formation from α -Pinene Ozonolysis, *ACS Earth Space Chem.*, 5, 487-
912 499, 10.1021/acsearthspacechem.0c00294, 2021.

913 Xu, L., Kollman, M. S., Song, C., Shilling, J. E., and Ng, N. L.: Effects of NO_x on the Volatility of Secondary
914 Organic Aerosol from Isoprene Photooxidation, *Environ. Sci. Technol.*, 48, 2253-2262,
915 10.1021/es404842g, 2014.

916 Yáñez-Serrano, A. M., Nölscher, A. C., Bourtsoukidis, E., Gomes Alves, E., Ganzeveld, L., Bonn, B., Wolff,
917 S., Sa, M., Yamasoe, M., Williams, J., Andreae, M. O., and Kesselmeier, J.: Monoterpene chemical

918 speciation in a tropical rainforest: variation with season, height, and time of day at the Amazon Tall
919 Tower Observatory (ATTO), *Atmos. Chem. Phys.*, 18, 3403-3418, 10.5194/acp-18-3403-2018, 2018.
920 Yáñez-Serrano, A. M., Bourtsoukidis, E., Alves, E. G., Bauwens, M., Stavrou, T., Llusà, J., Filella, I.,
921 Guenther, A., Williams, J., Artaxo, P., Sindelarova, K., Doubalova, J., Kesselmeier, J., and Peñuelas, J.:
922 Amazonian biogenic volatile organic compounds under global change, *Global Change Biology*, 26,
923 4722-4751, <https://doi.org/10.1111/gcb.15185>, 2020.
924 Ye, Q., Wang, M., Hofbauer, V., Stolzenburg, D., Chen, D., Schervish, M., Vogel, A., Mauldin, R. L.,
925 Baalbaki, R., Brilke, S., Dada, L., Dias, A., Duplissy, J., El Haddad, I., Finkenzeller, H., Fischer, L., He, X.,
926 Kim, C., Kürten, A., Lamkaddam, H., Lee, C. P., Lehtipalo, K., Leiminger, M., Manninen, H. E., Marten,
927 R., Mentler, B., Partoll, E., Petäjä, T., Rissanen, M., Schobesberger, S., Schuchmann, S., Simon, M., Tham,
928 Y. J., Vazquez-Pufleau, M., Wagner, A. C., Wang, Y., Wu, Y., Xiao, M., Baltensperger, U., Curtius, J.,
929 Flagan, R., Kirkby, J., Kulmala, M., Volkamer, R., Winkler, P. M., Worsnop, D., and Donahue, N. M.:
930 Molecular Composition and Volatility of Nucleated Particles from α -Pinene Oxidation between -50 °C
931 and $+25$ °C, *Environmental Science & Technology*, 53, 12357-12365, 10.1021/acs.est.9b03265, 2019.
932 Zhang, X., McVay, R. C., Huang, D. D., Dalleska, N. F., Aumont, B., Flagan, R. C., and Seinfeld, J. H.:
933 Formation and evolution of molecular products in α -pinene secondary organic aerosol, *Proc. Natl. Acad.*
934 *Sci.*, 112, 14168-14173, doi:10.1073/pnas.1517742112, 2015.
935 Zhao, J., Häkkinen, E., Graeffe, F., Krechmer, J. E., Canagaratna, M. R., Worsnop, D. R., Kangasluoma,
936 J., and Ehn, M.: A combined gas- and particle-phase analysis of highly oxygenated organic molecules
937 (HOMs) from α -pinene ozonolysis, *Atmos. Chem. Phys.*, 23, 3707-3730, 10.5194/acp-23-3707-2023,
938 2023.
939